

Article

Mass-Movement Causes and Landslide Susceptibility in River Valleys of Lowland Areas: A Case Study in the Central Radunia Valley, Northern Poland

Anna Małka ^{1,*} , Lesław Zabuski ² , Frieder Enzmann ³  and Arkadiusz Krawiec ⁴ 

¹ Branch of Marine Geology, Polish Geological Institute—National Research Institute, 5 Kościarska Street, 80-328 Gdansk, Poland

² Institute of Hydro-Engineering, Polish Academy of Sciences, 7 Kościarska Street, 80-328 Gdansk, Poland; leslawzabuski@ibwpan.gda.pl

³ Institute of Geosciences, Johannes Gutenberg-University Mainz, Johann-Joachim-Becher-Weg 21, D-55128 Mainz, Germany; enzmann@uni-mainz.de

⁴ Faculty of Earth Sciences and Spatial Management, Nicolaus Copernicus University, Lwowska 1, 87-100 Torun, Poland; arkadiusz.krawiec@umk.pl

* Correspondence: anna.malka@pgi.gov.pl

Abstract: This work aims to analyse the mechanisms and factors contributing to shallow soil landslides in river valleys entrenched in lowlands on the example of the Central Radunia Valley. The combination of susceptibility analysis using geographic-information-system-based statistical models, field surveys, analysis of archival materials, and numerical modelling for the analysis of slope stability and hydrogeological processes allows for comprehensive landslide reconstruction, mass movement mechanism description, and an explanation of the role of triggering and causal factors. The results emphasise the need for cross-disciplinary studies of shallow soil landslides. The identification and prioritisation of the causal factors indicate that geomorphological conditions play a particularly important role. The current study shows that the greatest influence on landslide formation in the Central Radunia Valley is slope angle, as determined using a high-resolution digital elevation model. The slope angle factor is sufficient to produce a reliable susceptibility map (the areas under the curve of the success rate and prediction rate curves are 87.84% and 85.34%, respectively). However, numerical modelling of slope failure also clearly indicated that there was a significant influence of anthropogenic impacts on the landslide process. We determined that the main triggering factor causing the January 2019 Rutki landslide was related to the drilling of a borehole on 10 January 2019. The water used for drilling hydrated the soil and thus weakened the stability conditions.

Keywords: mass movements; numerical modelling of landslides; landslide susceptibility; slope hydrology; lowland areas; Radunia Valley



Citation: Małka, A.; Zabuski, L.; Enzmann, F.; Krawiec, A. Mass-Movement Causes and Landslide Susceptibility in River Valleys of Lowland Areas: A Case Study in the Central Radunia Valley, Northern Poland. *Geosciences* **2023**, *13*, 277. <https://doi.org/10.3390/geosciences13090277>

Academic Editors: Jesus Martinez-Frias and Ioannis Koukouvelas

Received: 21 July 2023

Revised: 29 August 2023

Accepted: 30 August 2023

Published: 13 September 2023



Copyright: © 2023 by the authors. Licensee MDPI, Basel, Switzerland. This article is an open access article distributed under the terms and conditions of the Creative Commons Attribution (CC BY) license (<https://creativecommons.org/licenses/by/4.0/>).

1. Introduction

In Poland, people have been settling in river valleys since the Stone Age [1]. Over time, river valleys were strongly transformed during the industrialisation period. The main triggering factor responsible for the activation or reactivation of landslides is precipitation [2–5]. However, for landslides that develop in deeply entrenched river valleys, an additional trigger is the lateral erosion of the landslide toes (as shown in [6–10], to name but a few). Riverbank erosion, combined with the infiltration of rainwater into mobilised mass, makes near-river forms more susceptible to activation than slope landslides [11–14]. Nowadays, natural causative factors overlap with human activities, significantly increasing the risk of landslides. Due to the presence of conditioning (causal) and overlapping triggering factors, mass movements in entrenched river valleys result in significant financial losses, especially in places where there are hydroelectric power plants near a watercourse [15,16].

The basic tools for determining the causes of landslides and forecasting mass movements on a small scale are landslide susceptibility maps (LSMs) [17,18]. Approaches to and methods for assigning landslide susceptibility (LS) can be grouped into five broad categories, namely, (i) geomorphological mapping, (ii) analysis of landslide inventories, (iii) heuristic or index-based approaches, (iv) process-based methods, and (v) statistically based modelling methods [19]. However, the methods used in landslide susceptibility allow for the assessment of the role of anthropogenic factors to a limited extent [20], which is related to the difficulties caused by including factors that rapidly change in time and space in two-dimensional GIS analysis. Field surveys and stability analysis, as well as groundwater level and inclinometric monitoring, are carried out on individual landslides and, therefore, allow for the determination, to a greater extent, of the influence of anthropogenic actions on the activation and progression of landslides [21–25]. Such thorough research makes it possible to compare and supplement the conclusions resulting from susceptibility analyses.

This study primarily aimed to achieve (i) a comprehensive reconstruction of individual landslide development in a river valley entrenched in lowlands, (ii) the determination of anthropogenic triggering factors through the analysis of slope stability and hydrogeological processes, (iii) the identification and prioritisation of factors conditioning landslide development in river valleys entrenched in lowlands, and (iv) landslide susceptibility assessment using geographic-information-system (GIS)-based statistical models, i.e., logistic regression (LR).

This is the first study of the Central Radunia Valley, where the role of causal and triggering factors was determined, and LS was assessed. The determination of anthropogenic triggering factors was possible through the analysis of the slope stability and hydrogeological processes of the Rutki landslide. The numerical modelling of slope failure processes allows for a description of the mechanisms of shallow soil mass movement.

Study Area

The Central Radunia Valley (Babi Dół gorge) is located in a young morainic area in the northern part of the Polish Lowlands within the ice sheet limit of the Pomeranian Phase of the Vistulian (Weichselian) Glaciation (Figure 1) [26]. The study focuses on an area that occupies 4.75 km² and is approximately 4.5 km long and up to 1 km wide. The Babi Dół gorge is narrow and U-shaped, and it is oriented in a NE–SW direction. The Central Radunia Valley is characterised by a significant inclination (25–40°) as well as a high relief (25–35 m). The stream flow decline is substantial, at up to 6.8‰ [27], while the average gradient of the Radunia River is 1.62–1.64‰ [28].

The study area has a distinctly maritime climate. The average wind speeds are 3.7 m/s, and the prevailing winds are from the SW, W, and NW directions [29]. The average annual rainfall recorded at Bąkowo station was approximately 630 mm, with most rainfall occurring in July [30,31]. During the period between 1951 and 2015, the average annual air temperature recorded at Chojnice station was 7.1 °C. However, the seasonal average air temperatures are changeable, corresponding to 16.3 °C in the summer (with a maximum of 21.8 °C and a minimum of 11.4 °C) and −1.9 °C in the winter (with a maximum of 0.6 °C and a minimum of −4.1 °C) [32]. The study area has a fairly large number of mean annual frost (69) and ice (42) days [32].

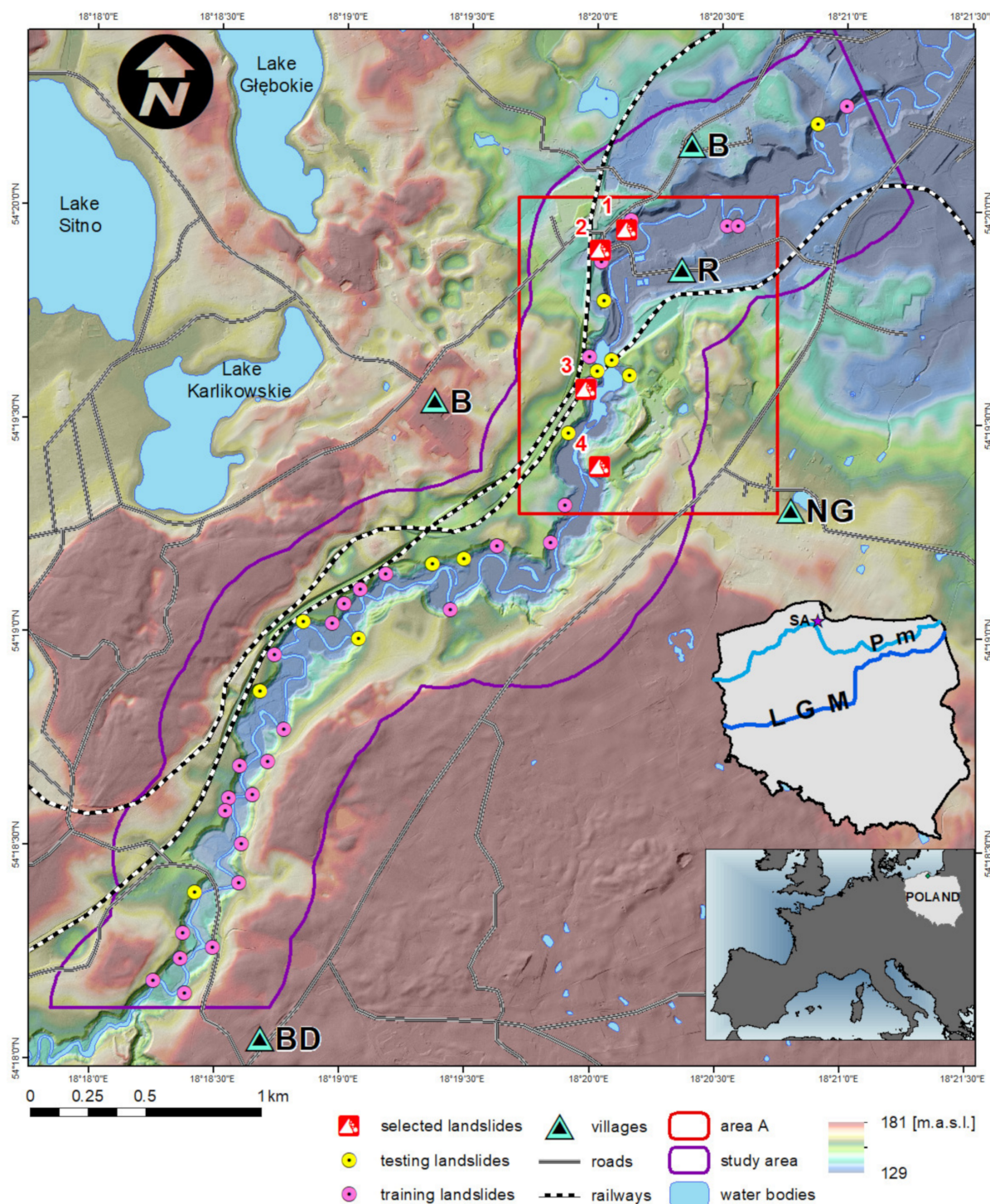


Figure 1. Location of the study area. Abbreviations: SA—study area, B—the village of Borkowo, R—the village of Rutki, NG—the village of Nowy Glińczę, BD—the village of Babi Dół, LGM—the Last Glacial Maximum ice sheet extent, and Pm—the Scandinavian Ice Sheet limits during the Pomeranian Phase (the glaciation extent according to Marks, 2012). Selected landslides—location of landslides described in text; training and testing landslides—location of landslides used in GIS analyses.

In terms of geomorphology, the study area is located within a small outwash plain [33,34]. The Radunia River Valley is polygenetic and consists of segments generated through different processes related to margin fluctuations of the Late Weichselian ice sheet [35]. It is located in a tunnel valley running NE–SW [33]. During the Late Vistulian, the tunnel valley was filled with blocks of buried dead ice, which protected against infilling with younger glacial and

postglacial deposits [36]. The dead ice blocks in the substratum acted as a dam for the waters upstream of the valley [35]. This resulted in the formation of oversteepened slopes, which occurred to an extent greater than in the other parts of the Radunia Valley. The geological structure of the study area is homogeneous, dominated by glaciofluvial sediments [33,34,37]. These deposits consist of yellow-brown medium- and fine-grained sand, fine gravel, and boulders. The sand layers are deposited horizontally and diagonally. Their thickness sometimes exceeds 20 m [33,34]. The tills appear in a small area in the southern part, near the village of Babi Dół [27]. The floodplain in the Central Radunia Valley is narrow, typically spanning several tens to about a hundred metres, and contains a few paleomeanders. It consists of fluvial deposits from the Holocene up to 6 m thick: sand and silt with organic matter, sometimes peat and peaty silt [34,37,38]. At the bottom of the valley, in the middle part of the study area, there is an erosional terrace resting about 5 m above the floodplain [34].

The Radunia River is fed mainly by groundwater and has an alpine character with a fast river current. The average annual value of the unit outflow for the Radunia catchment ranges from 8 to 10 $\text{dm}^3\text{s}^{-1}\text{km}^{-2}$ [31]. Such a large outflow affects the shape and depth of the groundwater table and increases river erosion. Data collected between 1963 and 2000 show that the water level in the Radunia River is at its highest in the winter and the early spring (February–April) and in the summer (July–September) [39]. The northern part of the research area has been anthropogenically altered. The Radunia River has been regulated, and, in the vicinity of Rutki, there is a dam reservoir. The hydroelectric power plant in Rutki influences the area's water regimentation. The power plant started operating in October 1910, and it has been generating electricity until now without any long breaks [40].

The 12 m high soil dam of the power plant has been secured with a retaining wall. At the end of the 20th century, slope processes resulted in the formation of numerous cracks in the retaining wall, which could damage the dam. In 1988, the soil-nailing method was used in stabilising the slope [41,42]. Over time, the dam reservoir has decreased in size due to sedimentation [27,43].

In the slopes of the Radunia River Valley, the depth to the groundwater table follows the topography and ranges from 3 to 25 m. The bottom of the river valley and the area near the hydroelectric power plant in Rutki are characterised by the shallow presence of the first unconfined aquifer, locally confined in the range of <5 m below ground level [44,45]. Underground water drains to the Radunia River in the north, which is manifested by its right-bank tributaries, located in the area of Babi Dół [46].

In the northern part of the study area, there are roads, many buildings, a railway line, and a historic truss bridge built by the Germans in the autumn of 1886. The railway line (Figure 1), which is part of the Coal Trunk-Line built between 1926 and 1933 [47], runs through the entire research area on the left side of the Radunia River.

The southern part of the research area, which is less anthropogenically changed, is located within the 'Jar Raduni' Nature Reserve. The aim of the reserve is to protect the unique ecosystems of the ravine section of the river. The ecosystems are mountainous in nature, with corresponding flora and fauna species. The area is covered in oak–hornbeam and riparian forests, which harbour saprobionts. The area's landslide processes have a significant impact on the ecosystems occurring in the reserve. In this region, there are rare lichens [48] and dead trunks that have fallen into the river. They create habitats for many plants and animals [49]. In the southern part of the Babi Dół gorge, landslides disturb water conditions and create a specific environment that significantly increases biodiversity.

2. Materials and Methods

Various research methods were used depending on the applied research scale (Table 1). Primary data were mainly used in this study. A field survey was conducted between January 2019 and January 2023. For the selected Rutki landslide, piezometers and inclinometers were installed. Secondary data (old maps, geotechnical documentation, and

precipitation data) obtained from different sources were collected and reinterpreted as well. The selected data made it possible to perform numerical, spatial, and statistical analyses.

Table 1. Methods and analyses used to delineate, identify, describe, and assess mass movement in the Babi Dół gorge with different scales.

| Scientific Research Methods | | | | | |
|-------------------------------------------------------------------------------------------------|------------------------------|--------------------------|--------------------------------------------|--------------------|------------------|
| | Analysis of Secondary Data * | Analysis of Primary Data | | | |
| | | Field Surveys | Drilling/ Inclinometers, Piezometers | Numerical Analyses | Spatial Analyses |
| Investigation of the Rutki landslide with a scale of 1:500 | X | X | X | X | X |
| Assessment of the landslide susceptibility of the Central Radunia Valley with a scale of 1:5000 | X | X | | | X |

* The secondary data come from the following sources: Polish National Geodetic and Cartographic Resources; Polish Geological Institute; Energa SA Group, Poland; INGEO Company, Poland; Provincial Road Authority in Gdańsk, Poland; Berlin State Library, Germany; the Internet.

2.1. Analysis of the Rutki Landslide

The Rutki landslide (Figure 1—landslide 2) was studied in detail. Archival materials were used for the landslide's description and analysis, including situation plans and topographic as well as geological maps from the 19th and early 20th centuries [37,50–53]. Secondary data from geotechnical documentation from the early 21st century [38,54] were reinterpreted. The Rutki landslide has been observed since the 13 January 2019. The geomorphological surveys and analysis of archival materials allowed for the reconstruction of the old landslide and the main sliding surface.

Furthermore, observations of water levels in the Radunia River carried out between 1995 and 2020 and precipitation data from between 2005 and 2020 provided by Energa SA Group were taken into account. In order to determine the depth of the groundwater table, piezometric monitoring using four shallow piezometers (P1, P2, P3, P4) to a depth of 4 m (since September 2019) and two deeper piezometers (RP1, RP2) to a depth of 24 m (since October 2021) has been carried out. To determine the magnitude, rate, direction, depth, and type of landslide movement, measurements of the underground displacement of slopes using two inclinometers (RI1, RI2) via an RST MEMS digital inclinometer probe with a measurement interval of 0.5 m have been carried out since November 2021. The entire apparatus consists of a probe, a heavy-duty control cable wound onto a slip-ring reel, and KLION software (SISGEO, <https://www.sisgeo.com/company.html>; accessed on 10 January 2023).

The geological structure of this area was determined primarily on the basis of a newly drilled borehole (up to 24 m) and a formerly drilled borehole (whose details were obtained from secondary data) (up to 60 m). Finally, a geological cross-section for the Rutki landslide was drawn to better understand the morphology and to reveal the underlying geology.

To illustrate the characteristics, parameter measurements, and track changes in the dynamics of displacements in the Rutki landslide, two airborne-laser-scanning (ALS) datasets and one terrestrial-laser-scanning (TLS) dataset were used. ALS and TLS make it possible to create high-resolution digital terrain models (DTMs) and perform multi-temporal analyses [55,56]. The first ALS ISOK (Pol. Informatyczny System Osłony Kraju) dataset comes from the open source digital dataset of the National Geodetic and Cartographic Resources (<https://www.gov.pl/web/gugik>; accessed on 10 January 2023) and was collected on 6 April 2012 with a Leica ALS70 laser scanner. The second TLS was collected on 12 November 2019 and was acquired manually by the Polish Geological Institute–National Research

Institute using a Riegl VZ400 scanner. The third ALS dataset was acquired on 23 November 2021 by MGGP Aero company (<https://www.mggpaero.com/en/company.html>; accessed on 10 January 2023) using a Riegl VQ-480I scanner. The DTM made it possible to acquire landslide profiles at three time intervals.

As part of the analytical studies, the landslide process in Rutki was simulated using the FLAC2D (Fast Lagrangian Analysis of Continua) computer program based on the finite difference method (<https://www.itascacg.com/software/flac2d>; accessed on 10 January 2023) [57]. For the modelling of large displacements and for the observation of the landslide shape changes during movement, Lagrange formalism was adopted in simulation. The program employed calculates stress and deformations (displacements) in two dimensions (2D), determines the state (elastic, plastic), failure mode (shear, tension) in each zone or in the nodal point.

2.2. Susceptibility Assessment of the Central Radunia Valley

The first step was to confine the research area to one geomorphological element, i.e., a homogeneous section of the river valley entrenched in lowlands (Figure 1). The corresponding analysis was limited to the sander area on either side of the river, approximately 500 m from the upper edge of the valley. Geomorphological mapping was performed to develop an inventory map of landslides and identify the mechanism of landslide movement. In the interpretation of the landslides, shaded models of the terrain surface (hillshade) and topographic attributes generated from high-resolution (0.5×0.5 m) LiDAR (Light Detection and Ranging) data from 2012 were also prepared. Based on the digital elevation model (DEM) analysis and field work carried out between 2019 and 2020, a map of landslides with a scale of 1:5000 was developed, and it served as the primary source of information for susceptibility assessment. Only active landslides were taken into account in the analysis.

A training sub-dataset and thematic maps were used to develop a training model, while another (testing) sub-dataset was used for validation. As stressed by Chung and Fabbri [58], random partitioning is a mandatory step in prediction modelling. Firstly, the landslide dataset (100% including 44 active landslides) was divided into training and validation sub-datasets, covering 70% and 30% of all active landslides, respectively (Figure 1). Secondly, the landslides were presented as a grid of points marked every 10 m. In total, 847 points were used. The same number of points was selected randomly from the landslide-free area [59]. Landslide inventory and 25 conditioning factors were prepared for susceptibility modelling (Table 2).

The research considered geological, geomorphological, hydrological, and anthropogenic predisposing factors (Table 2). All geo-factors were obtained via the further processing of the original data.

Geomorphological and hydrogeological factors were calculated from ALS ISOK datasets. The point density within the ALS-based point cloud was 4 points/m^2 . The new aspect proposed in this study is the use of a modified digital elevation model (MDEM), which allows for the inclusion of the extent to which buildings influence the runoff of water in the model. The first ten topographic attributes were calculated from the DEM, while the rest were calculated from the MDEM (Table 2). The NDVI index was prepared based on SENTINEL-2 satellite imagery with a scale of 1:10,000 from 14 June 2020 (Table 2). A land use and land cover map was prepared using the topographic object database, the DEM and aerial photos. The lithology layer was developed by generalising geological formation from a detailed geological map with a scale of 1:50,000 [33,34]. In order to refine geological boundaries, the DEM, up-to-date drilling data, and field surveys were used. The resolution (pixel/grid size) of all the raster maps used in the analysis was 1×1 m. Then, the classification and regression trees (C&RT) were calculated to assess the importance of individual conditioning factors. To identify factors that were overly correlated with each other, principal component analysis (PCA) was performed, for which a variable correlation matrix was used (TIBCO; <https://docs.tibco.com/data-science/textbook>; accessed on 10 January 2023).

Table 2. Spatial digital data used in GIS analysis.

| Digital Data | Source | Thematic Layers | Websites |
|----------------------------------------|--------------------------------------------------------------------------------------------------------------------------------|--------------------------------------------------------------------------------------------------------------------------------------------------------------------------------------------------------------------------------------------------------------------------------------------------------------------------------------------------------------------------------------------------------------------------------------------------------------------------------------------------------------------------------------------------------------------------------------------------------------|----------------------------------------------------------------------------------------------------------------------------------------------------------------------------------------------------------------------------------------------------------------------------------------------------------------------------------------------------------------------------------------------------------------------|
| | DEM*, field surveys*, engineering documentation*, scientific publications*, Google Earth™ imagery*, interviews with residents* | Landslide inventory | https://www.pgi.gov.pl/gdansk/projekty-krajowe/osuwiska-doliny-raduni.html *; accessed on 10 January 2023 |
| Digital elevation model (DEM) | National Geodetic and Cartographic Resources, Poland | The topographic attributes: slope angle, slope height (SH), profile curvature, plan curvature, convergence index (CI), length slope factor (LS), topographic position index (TPI), valley depth (VD), slope mean of upslope area (SMUA), terrain ruggedness index (TRI), digital surface model (DSM), DSM insolation (DSMI), modified digital elevation model (MDEM), channel network base level (CNBL), SAGA catchment area (SCA), SAGA catchment slope (SCS), SAGA topographic wetness index (STWI), flow path length (FPL), stream power index (SPI), MDEM insolation (MDEMI), geomorphons, aspect | https://www.gov.pl/web/gugik ; accessed on 10 January 2023 https://www.geoportal.gov.pl ; accessed on 10 January 2023 https://www.pgi.gov.pl/gdansk/projekty-krajowe/osuwiska-doliny-raduni.html *; accessed on 10 January 2023 |
| Topographic object database (BDOT 10k) | National Geodetic and Cartographic Resources, Poland DEM*, field surveys* | Land use and land cover (LULC) | https://www.gov.pl/web/gugik ; accessed on 10 January 2023 https://www.geoportal.gov.pl ; accessed on 10 January 2023 https://www.pgi.gov.pl/gdansk/projekty-krajowe/osuwiska-doliny-raduni.html *; accessed on 10 January 2023 |
| Digital geological data | Polish Geological Institute, National Research Institute [33,34]; DEM*, field surveys* | Lithology | https://geologia.pgi.gov.pl ; accessed on 10 January 2023 https://www.pgi.gov.pl/gdansk/projekty-krajowe/osuwiska-doliny-raduni.html *; accessed on 10 January 2023 |
| SENTINEL-2 satellite imagery | Sinergise Laboratory for geographical information systems Ltd., Slovenia | Normalised difference vegetation index (NDVI) | https://www.sentinel-hub.com https://www.pgi.gov.pl/gdansk/projekty-krajowe/osuwiska-doliny-raduni.html *; accessed on 10 January 2023 |

* The sources were individually consulted as part of this study.

Landslide susceptibility maps were developed using logistic regression. This multivariate statistical method is a standard statistical model for LS assessment [20,60–65]. The LR method was selected because of its greater reliability compared to other methods of susceptibility assessment; this aspect has been confirmed by many results of verification using ROC curves [66–68]. Furthermore, considering other studies on young morainic areas [20,69], it is expected that these models are suitable for achieving highly accurate landslide modelling at the regional level. This method is based on the following formula:

$$P = \frac{1}{1 + e^{-z}} \quad (1)$$

In Equation (1), P is the probability of a landslide's occurrence and varies from 0 to 1 on an s-shaped curve, while z represents a linear logistic model and varies from $-\infty$ to $+\infty$. The linear logistic model was defined as

$$z = \beta_0 + \beta_1 X_1 + \beta_2 X_2 + \dots + \beta_n X_n \quad (2)$$

In Equation (2), β_0 is the intercept of the model (constant), n is the number of independent variables, β_i ($i = 1, 2, 3, \dots, n$) is the regression coefficient of the model, and X_i ($i = 1, 2, 3, \dots, n$) is the independent variable [63,70]. Validation of the predictive model is a crucial step in landslide susceptibility mapping [71]. The performance of the susceptibility model was evaluated using the success and prediction rate criteria developed by Chung and Fabbri [58]. The areas under the curve (AUC) of the success rate curve (SRC) and prediction rate curve (PRC) plots are a quantitative measure used to estimate a model's quality [58,72]. The AUC for SRC represents the ability of a susceptibility model to reliably classify the occurrence of existing landslides, whereas the AUC of PRC explains the capacity of a proposed landslide model to predict landslide susceptibility [73]. The following programs were used to calculate the conditioning factors of landslides and perform the landslide susceptibility analysis: SAGA 7.9.0, ARCGIS 10.3.1, Global Mapper 18.0, and Statistica v.13.0.

3. Results

3.1. Landslides in the Central Radunia Valley

Until this study, landslides in the Central Radunia Valley have not been the subject of wider scientific consideration. During the field surveys, 73 landslide forms with a total area of 286,800 m² were identified in the research area. About 60% of them have been active in recent years, with their activity manifesting in the form of broken or fallen trees and distinct river abrasion caused by the undercutting of slopes. All landslides were characterised by steep slopes (20–66°). The vast majority of them covered the entire slopes from their upper edge to the bottom of the valley. Mass movements were retrogressive, and they caused the recession of the upper edges of the slopes. The largest landslides affected an area of 10,000–20,000 m². However, smaller landslides, with a surface area equal to 200–300 m², were more prevalent. The average size of a landslide was 3900 m² (median = 2100 m²). The main scarps were quite distinct and varied in height from 1 to 6 m. Most of them occurred in the concave banks, and this can be associated with the presence of toe erosion.

The slope failures in the study area were classified during field surveys considering material and movement type based on the modified Varnes' landslide classification [74–76]. Earth (soil) slide, earthflow (wet and dry), or combined complex earth slide and earthflow were predominant (Figure 2).

The active character of the landslides in this area was noticed in the 19th century. In the situational plan of the Radunia River, the chevrons mark the fragments prone to slope movement [52]. Furthermore, the previously used geoenvironmental solutions indicate that as early as in the 19th century, builders and engineers were already aware of the presence of landslides. In the area of the truss bridge built in 1886, there is a structure directing the flow of water along the slope (Figure 2a) (similar solutions have been applied today to stabilise the landslides in Borkowo and Rutki (Figure 2d,f)).



Figure 2. Examples of landslides and engineering countermeasures for landslide disaster mitigation in the Radunia Valley. For more details on the locations, see Figure 1. (a) Landslide 3 near Borcz—old drainage channels, June 2020 (photo taken by Małka); (b) landslide 4 near Nowy Glińcz—an earthflow that developed due to water runoff from excavation, April 2013 (photo taken by Trojanowska); (c) landslide 1 in Borkowo—an earth slide and earthflow, February 2013 (photo taken by Cirocki); (d) stabilisation of landslide 1 in Borkowo, March 2022 (drone photo taken by Maciaszek); (e) landslide 2—an earth slide and earthflow in Rutki, February 2019 (photo taken by Małka); (f) stabilisation of landslide 2, June 2021 (drone photo taken by Maciaszek).

Then, in 1910, during the construction of the hydroelectric power plant in Rutki, active landslides were observed in the area of the artificial reservoir, which were documented by archival photographs available in the power station. Subsequently, field work carried out in the area in the second half of the 20th century indicated mass movements [27]. Interviews

with the local residents showed that landslides had been occurring there ‘as long as they remember’, e.g., in 1980, a landslide in Borkowo (in the area of today’s kayak mooring) occurred, destroying the road and reaching the river.

Reviews of the documents and several site visits conducted between January 2019 and November 2022 indicated that mass movements in the Radunia Valley had been activated many times. There had been several landslide activation periods in this area: in April 2013, August 2013, and January 2019 (Figure 2b,c,e). These landslides caused significant damage to infrastructure (the destruction of the local and national road as well as breaks in and disruptions to the operation of the hydroelectric power plant in Rutki). They had a destructive effect on not only infrastructure but also the natural environment (consisting of the pollution of the river and the devastation of trees).

The April 2013 landslide (Figure 2b) was associated with the exploitation of the aggregate in the gravel pit. Near the upper edge of the valley in the central part of the research area near Nowy Glińcz, a deep mining pit was made. The pit then filled with rainwater, resulting in flows that partially filled the gorge with sand and silt. At that time, three earthflow fans, which silted the power plant reservoir, were documented in the river bed. Another landslide that damaged the local road occurred in August 2013 (Figure 2c). During the reconstruction of the road in 2010, an artificial depression was created, causing the accumulation of rainwater. This may have contributed to the change in the direction of groundwater runoff and the activation of the landslide. The Rutki landslide, described in detail in this paper, occurred in January 2019 during horizontal-borehole-drilling activities (Figure 2e).

3.2. An Example of Anthropogenic Causes of the Rutki Landslide

3.2.1. Description of the Landslide’s Development and Structure

The date of the formation of the landslide in Rutki is not known, but old maps indicate that gullies existed there in the early 19th century (Figure 3a) [50,51]. In the second half of the 19th century, a small landslide was active on the outer side of the river’s meander (Figure 3b) [52]. By the early 20th century, mass movements and linear erosion overlapped (Figure 3c) [37,53]. The analysis of old maps [37,51–53], geotechnical documentation [38], and the current field surveys indicated that there were multiple changes in the outflow of surface water, groundwater, and the location of springs associated with the anthropogenic changes in land use and the appearance of landslides (Figures 3 and 4).

At the beginning of the 20th century, a watercourse flowed through the area of the present landslide (Figure 3c). During the construction of the Coal Trunk-Line in the Rutki area between 1926 and 1933, a track bed was drained, which allowed for targeted flow and the infiltration of water into the ground. In an attempt to drain the area, a culvert was built to the north of a previously existing gully with a periodic watercourse [37,51,53] and also in the vicinity of the present main scarp of the landslide (Figures 3c and 4). Furthermore, concrete rings were put in, through which water flowed into the river. Over time, intensive sedimentation processes resulted in the culvert being clogged.

In 1910, 200 m south of the village of Rutki, the aforementioned power plant started operating. The hydroelectric reservoir retained the sediments. The water flow, which was free of sediments, had greater energy and caused increased erosion on the left, concave bank behind the power plant. As evidenced by an interviews with the inhabitants, an older Rutki landslide had been reactivated in this area in the 1970s.

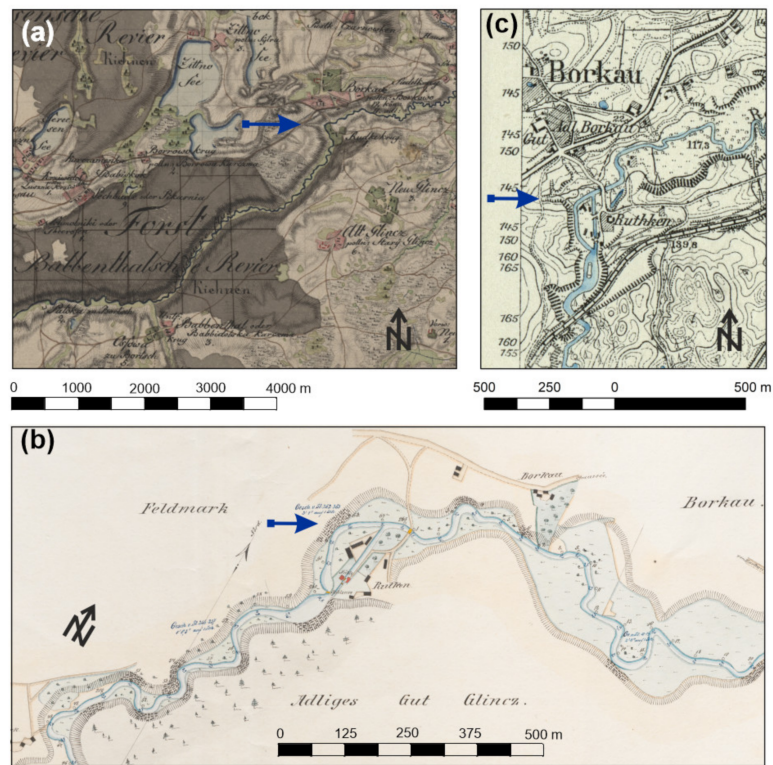


Figure 3. The Rutki landslide, indicated by three dark-blue arrows: (a) An old Schrötter topographic map with a scale of 1:50,000 dating from 1796 to 1802 (Berlin State Library, Berlin, Germany). (b) Radunia River situation plan from 1859. At that time, there was a watermill (Ger. Mühle) in the area of the current hydroelectric power plant in Rutki (State Archive in Gdańsk, Gdańsk, Poland). (c) An old topographic map, Messtischblätter, with a scale of 1:25,000 from 1900 (Berlin State Library, Germany) [50,52].

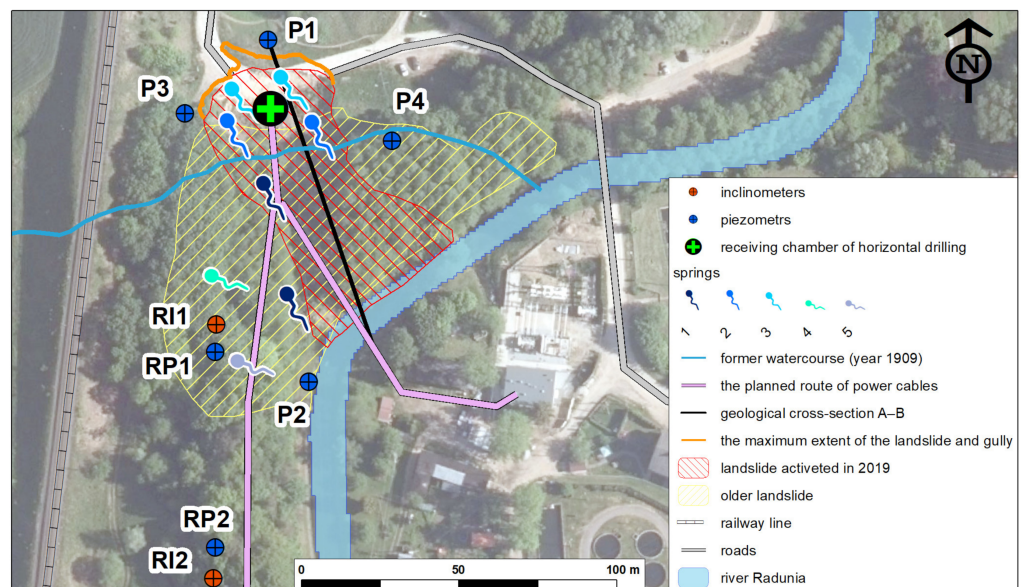


Figure 4. Location of the Rutki landslide and springs documented between 2018 and 2023. Springs: 1—documented in 2018, 2—documented between 2019 and 2020 (until landslide stabilisation), 3—documented in February 2019, 4—documented between 2018 and 2020 (until landslide stabilisation), and 5—documented between 2018 and 2023. P1, P2, P3, and P4—piezometers to a depth of 4 m; RP1—piezometer at a depth of 7.9 m; RI1—inclinometer at a depth of 8.3 m; RP2—piezometer at a depth of 23.9 m; RI1—inclinometer at a depth of 24 m.

The Rutki landslide reactivated on 10 January 2019 at 3 p.m. (Figure 1—landslide 2; Figures 4–9) (more photos of the landslide in Rutki can be found at <https://www.pgi.gov.pl/gdansk/projekty-krajowe/osuwiska-doliny-raduni.html>; accessed on 10 January 2023). Precipitation did not have any influence on the initiation of the landslide, as in the period directly before its development between the 7th and 10th of January 2019, a precipitation level of 4.6 mm was registered at the meteorological stations in Rutki. The main triggering factor consisted of phenomena related to the drilling of a borehole on 10 January 2019. On the day of the failure, horizontal drilling was performed during the installation of an underground power line between the plant and the village of Borkowo (Figure 4). In the area of the present landslide, the drilling was carried out at a depth of 2–3 m, and the drilling diameter was 30 cm. On the day of the incident, this drilling pierced the receiving chamber (Figures 3 and 7a).

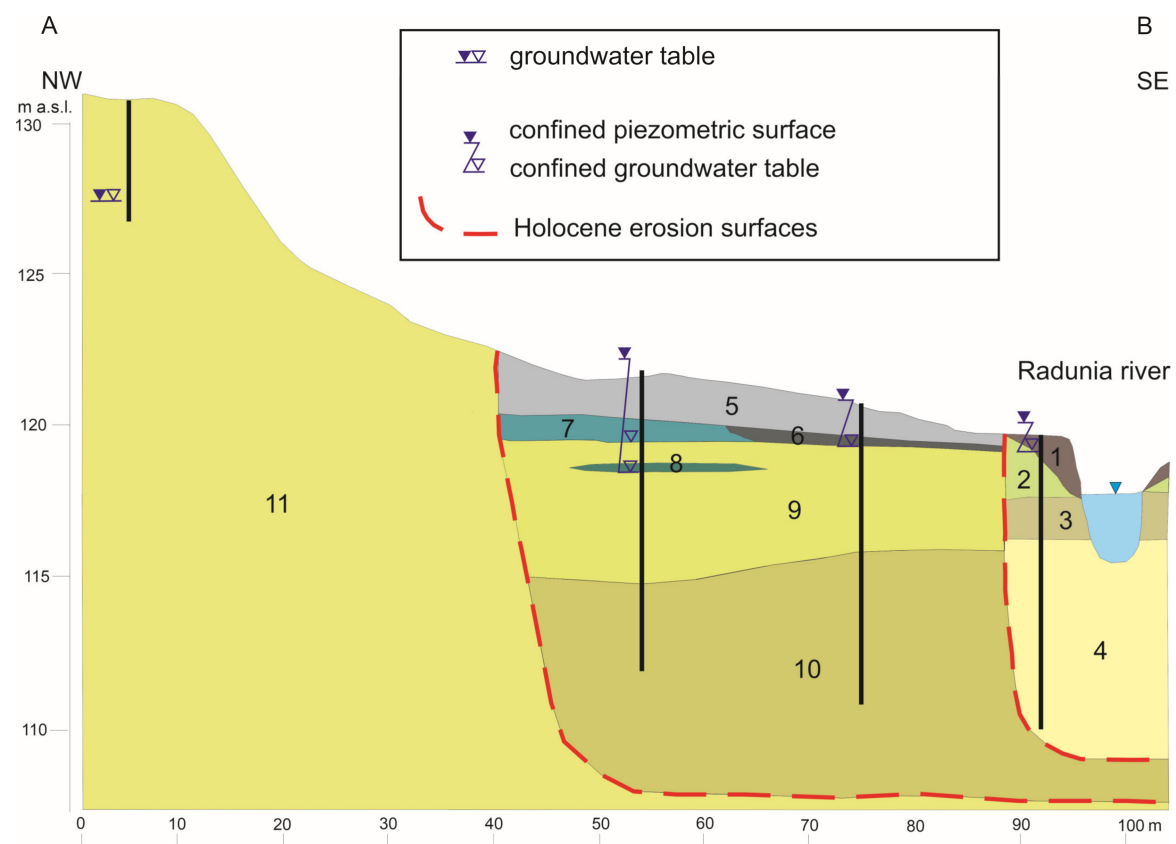


Figure 5. Schematic of geological cross-section (A–B) before 10 January 2019. Holocene: 1—river embankment, 2—sand, 3—gravel, 4—medium- and fine-grained sand, 5—humic sand, 6—peat, 7 and 8—organic silt, 9—fluvial sand, 10—fluvial gravel and sand; Pleistocene strata: 11—fluvio-glacial sand and gravel.



Figure 6. View of the upper zone (main scarp) of the landslide (Photo Zabuski; 10 January 2019).



Figure 7. (a) Image of the area one hour before the landslide occurred. In the foreground—horizontal drilling receiving chamber; in the background—the hydroelectric power plant in Rutki (Photo TELWENT; 10 January 2019, 2 p.m.). (b) Inflow of soil into the Radunia River (Photo Zabuski; 10 January 2019). (c) Drainage blockade—a buried culvert under the tracks and a clogged concrete circle (Photo Małka; 7 February 2019). (d) Gully erosion above main scarp along the slightly steep road (Photo Sreberski; 12 June 2019).

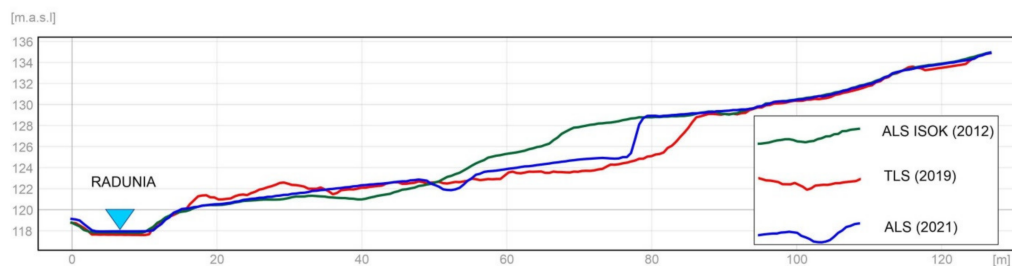


Figure 8. The longitudinal topographic profiles of the Rutki landslide. Abbreviations: ALS ISOK (2012)—dataset acquired through airborne laser scanning from the ISOK project collected on 6 April 2012 (pre-slide slope); TLS (2019)—dataset acquired through terrestrial laser scanning collected on 12 November 2019 (shortly after the failure); ALS (2021) dataset acquired through airborne laser scanning acquired on 23 November 2021 (after the stabilisation).

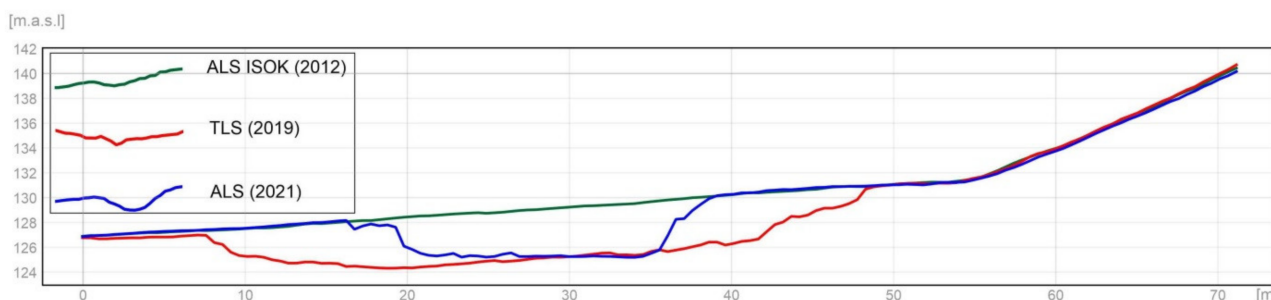


Figure 9. The parallel topographic profiles of the Rutki landslide. For an explanation of the abbreviations, vide Figure 8.

The initiation of the landslide was preceded by a noisy crash, followed by a landslide movement of approximately several meters per second (the whole process lasted only several seconds). Before the slide, an uplift was observed in the upper part of the slope surface. The uplift produced the rotational shape in the upper part of the slide. Evidence (the drillers' accounts) indicates that the landslide developed from its crown (main scarp) and moved towards the river (Figure 5). As a consequence of this movement, the surface was folded and undulated. These folds were successively denuded by flowing water over several days. The heavily hydrated soil masses finally reached the river (Figure 7b). Preventive measures were immediately implemented to prevent the formation of a dam by the soil. The landslide resulted in damage to the road constructed of concrete slabs, two electricity poles, a van, a power-generating unit and several other things (Figure 7b).

The dimensions of the landslide are given in Table 3. According to the modified Varnes' landslide classification [74–76], it can be described as a complex earth slide and earthflow.

Table 3. Dimensions of the Rutki landslide according to the terminology used by Dikau et al. [77].

| No. | Dimensions | [m] | Measurement Type |
|-----|--------------------------------------|-----|--------------------------------------------|
| 1 | Width of the displaced mass | 55 | Direct—measured on 13 January 2019 (field) |
| 2 | Length of the displaced mass | 85 | Direct—measured on 13 January 2019 (field) |
| 3 | Maximum depth of the displaced mass | 6 | Numerical model (Figure 13) |
| 4 | Height of the displaced mass | 4 | Direct—measured on 13 January 2019 (field) |
| 5 | Average depth of the failure surface | 2 | Numerical model (Figure 13) |
| 6 | Height of the main scarp | 4 | Topographic profiles (Figures 8 and 9) |

The Rutki landslide is an example of the influence of anthropogenic factors on movement initiation and progression. However, the original causal factors that governed the landslide's development were complex, among which topography, hydrology, and hydrogeology are the most essential.

The water level fluctuations were relatively significant, which was related to the alpine character of the Radunia River. The average water level in the 1995–2020 timeframe amounted to 117.97 m a.s.l., but water fluctuations in the Radunia River reached 1.79 m. The highest daily level (118.80 m a.s.l) occurred on 16 July 2017, while the lowest (117.01 m a.s.l) was recorded on 14 January 2004. Sudden fluctuations resulted from the alternating emptying and filling of the water reservoir of the power plant.

It is noteworthy that the geological structure was prone to landsliding (Figure 5). The slopes in the area of the landslide were steep (22–40°), which is related to the unique glacial origin of this area. The Central Radunia Valley is built mainly of low strength strata, i.e.,

non-cohesive soils. The slope in the area where the landslide occurred was composed of medium- and fine-grained sand, fine gravel, and boulders of glaciofluvial origin from the Weichselian glaciation. The thickness of this stratum in the old landslide body (colluvium) was more than 8 m (Figure 4, RP1); 50 m south of the landslide, it exceeded 24 m (Figure 4, RP2). In the vicinity of the river, there were fluvial sediments composed predominantly of sands and gravels interbedded with organic silts and peats of the Holocene. Within the fluvial sands, there were layers of organic silts (Figure 5). Thin, silty strata were closely associated with the sliding surface, which was listric (curved or spoon-shaped).

Previous borehole investigations (drilled before the catastrophic 2019 failure) indicated the presence of a pressurised groundwater system bounded by impermeable layers [38]. The underground water table lay at a relatively shallow depth and had an artesian character (Figure 5). Organic silts that occurred at a depth of 1.5–3.30 m b.g.l and peats that occurred at a depth of 0.5–1.3 m b.g.l formed an aquitard that confined the groundwater zone (Figure 5).

The analysis of geotechnical documentation [38] and the current field surveys indicate multiple changes in the location of the springs after the reactivation of the landslide in 2019 (Figure 4). After the failure, new ponds and springs formed on the slide. Moreover, the soil mass was considerably hydrated (Figures 2e, 6 and 7b). New springs were created in the slope (springs 2 and 3, Figure 4). However, the two newly formed springs (springs 2, Figure 4) existed until the landslide was stabilised; March–May 2020). During the field survey (7 February 2019), a short-term appearance of two springs was also observed within the main scarp. The springs, however, disappeared after a few weeks (springs 3, Figure 4).

Some evidence, such as new outflows from the main scarp and the widening of the damaged space above the crown, suggests that the landslide developed slowly after reaching temporary stability. In the period between January and September 2019, the retrogressive evolution of the main scarp was observed (Figure 7d). This enlargement of the landslide was mainly related to short gully erosion (about 10 m long) above the main scarp and along the slightly steep road (Figures 4 and 7d).

The difference between the original and final (landslide) surfaces can show the type and mechanism of mass movements (slide-flow) (Figures 8 and 9). On the upper part of the slope, the rotational slide induced a concave shape of the final surface, while in the lower part, it inclined from 0 to 6° towards the river, and the shape of the surface was convex or almost linear. The significant difference between the volume of the material in the upper and lower parts of the landslide (Figure 8) can be explained by the phenomenon of soil detachment from the riverbed (Figure 7b).

Following the formation of the landslide, groundwater monitoring via four piezometers has been carried out since 23 September 2019 (Figure 4). Measurements that were carried out until February 2020 showed a groundwater level to the north of the main scarp at an average depth of 3.63 m, 1.34 m in the eastern part, and 0.47 m in the toe in the immediate vicinity of the Radunia River. In March 2020, the stabilisation of the landslide began. This included drainage and the restoration of the culvert (Figures 2f and 7d). As a result, there was a significant drop in the groundwater level in the area of the landslide, e.g., in the case of piezometer 4, the groundwater table dropped, on average, by 0.46 m (max. 0.60 m). After the stabilisation of the landslide (Figures 2f, 8 and 9), higher groundwater fluctuations, ranging up to 0.31 m, were observed only in piezometer RP1.

The western, older part of the Rutki landslide currently monitored by inclinometer RI1 and piezometer RP1 matches the area active in the 19th century (Figure 3b). Inclinometric measurements that have been carried out since November 2021 show that within the unprotected older part of the Rutki landslide (inclinometer RI1), there is a creep up to a depth of approximately 2 m with a velocity of about 0.5 mm/month (Figure 10a,b).

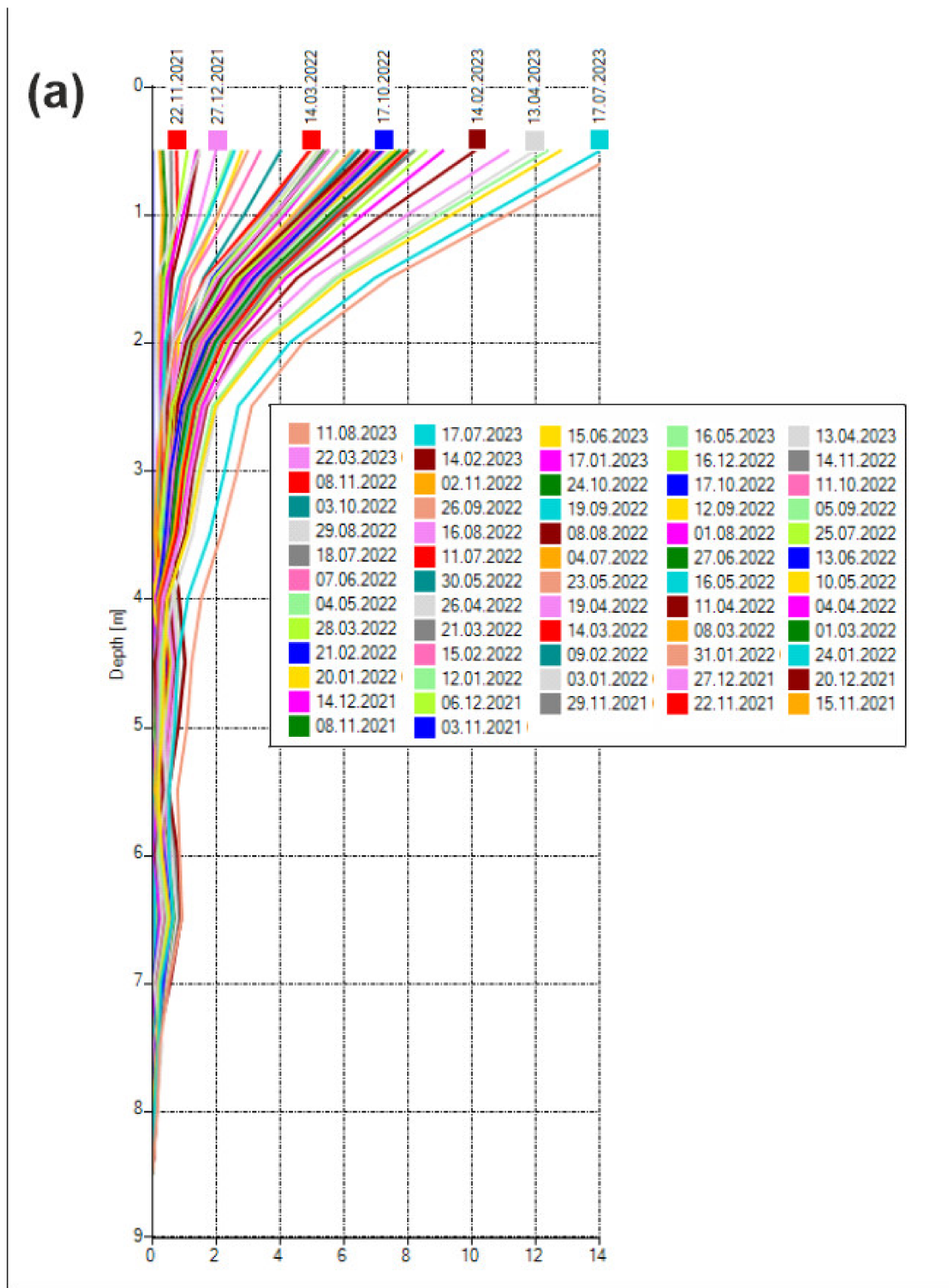


Figure 10. Cont.

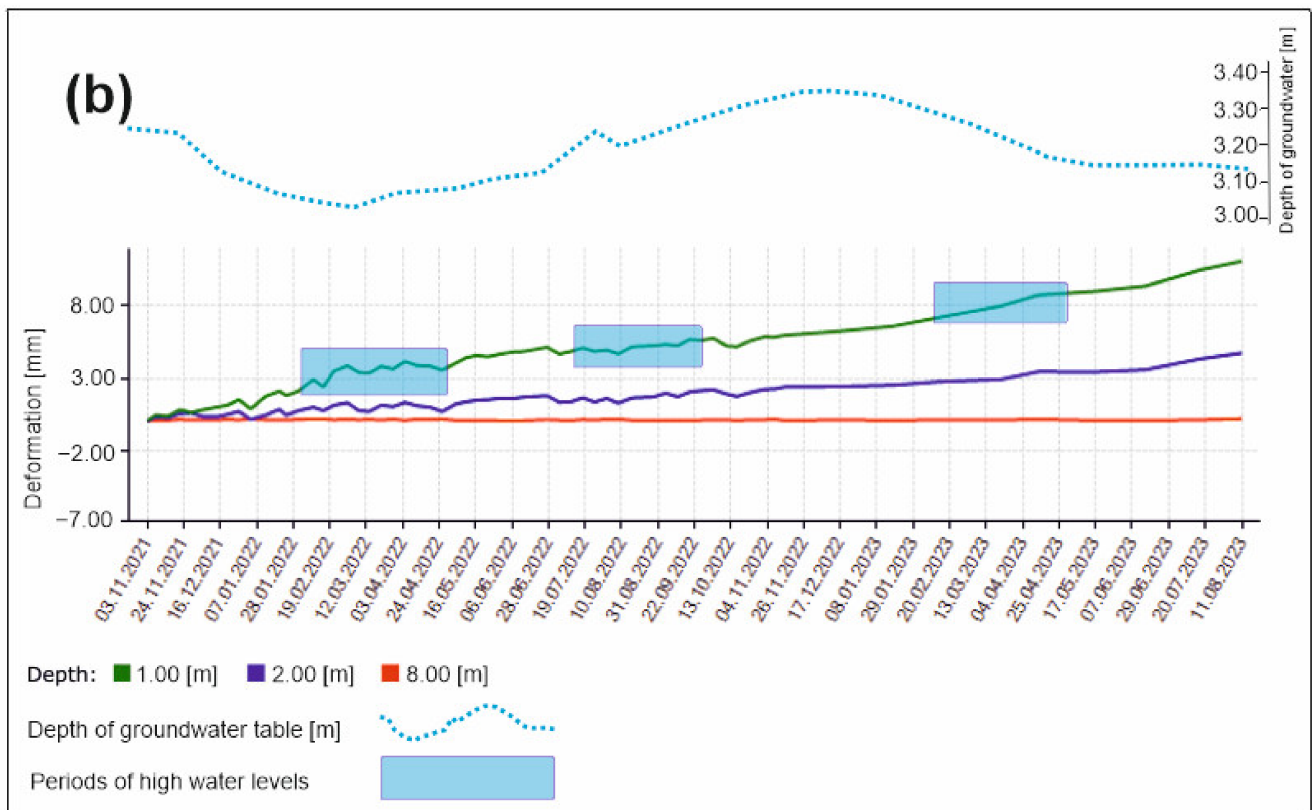


Figure 10. Measurements of changes in landslide movement at inclinometer RI1 and piezometer PI1: (a) curves of cumulative displacement; (b) horizontal displacements, depth of groundwater table, and periods of high river water levels as functions of time.

Groundwater (piezometer RP1) occurs here at a depth of about 3 m (Figures 4 and 10). Creeping occurs most rapidly during the winter and the early spring period, ranging from January to April. During this period, higher groundwater and higher river water levels occur as well (Figure 10b). No changes were observed for the second inclinometer (RI2), where groundwater occurs at 21 m (piezometer RP2; Figure 4).

3.2.2. Numerical Analysis of the Landslide’s Development Elaboration of the Landslide Model

Geomechanical and numerical models were constructed, and the landslide process was simulated [57] for the cross-section of the original slope (Figure 8). The models were divided into finite element zones (Figure 11), and meshes were created in consequence; examples of Model I and Model II are shown in Figure 12.

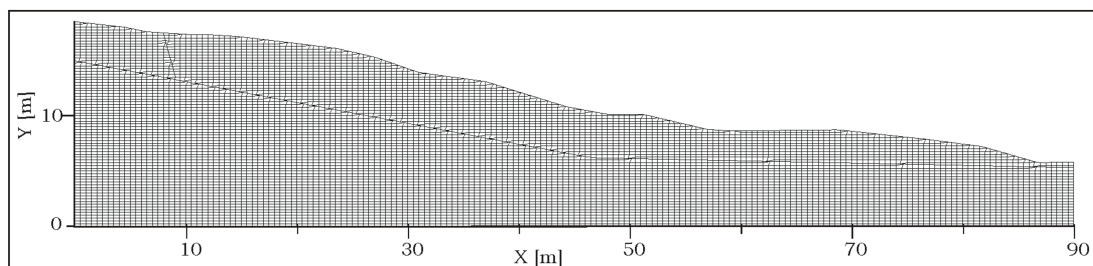


Figure 11. Finite difference (FD) mesh of the Rutki landslide via FLAC2D software [57].

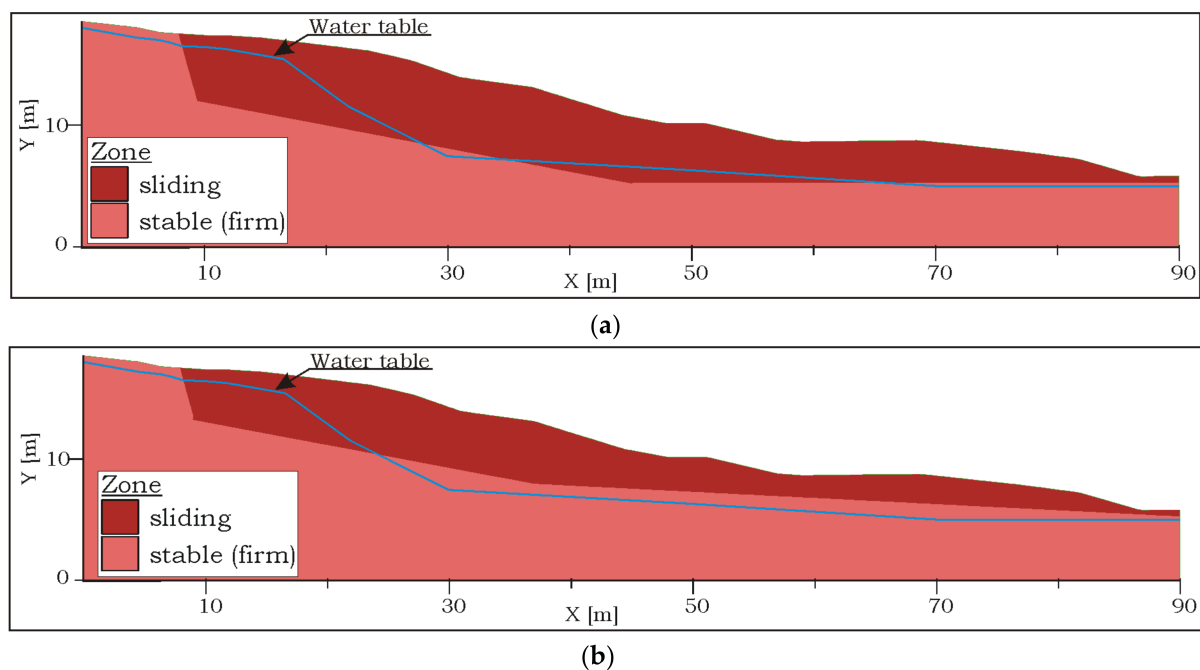


Figure 12. Division of the model into layers: (a) Model I—water table above the slip surface, where the landslide thickness is greater; (b) Model II—water table below the slip surface, where the landslide thickness is smaller.

The slope in Rutki is composed of sand, i.e., homogeneous soil without cohesion. Originally it was stable. However, water accumulated in the uppermost zone of the slope (Figure 12) as it was pumped into the borehole during the horizontal boring. The water infiltrating into the soil caused a sudden increase in pressure. The solid ground became liquefied by the saturation with water, and the soil behaved like a liquid, exhibiting almost no shear strength (so-called quicksand).

Results of the Landslide Simulation

As the Lagrange approach was used, large displacements are visible as a result of progress in the numerical simulation process. The landslide movement was not stabilised in the iteration procedure but was stopped in an arbitrary way. Some characteristic processes and deformations can nevertheless be observed. Furthermore, a slide in the upper part of the slope appeared. Two slide zones, both in Model I and II, are depicted in Figure 13a,b.

The first slide zone in both Model I and Model II is approximately in alignment with the location of the silt layer and the probable main sliding surface (Figure 5).

A very significant change of the slope shape resulting from the movement can be observed when the displacement field is rendered more prominent via double multiplication (Figure 14). The execution of further numerical simulations was impossible due to numerical constraints.

Figure 14 shows that a large displacement appeared on the upper part of the slope.

However, in the more advanced stage of the slide, the soil can move continuously and cover the lower part of the slope, lying between coordinate $X = 50 \div 60$ m and the river (see Figure 14b).

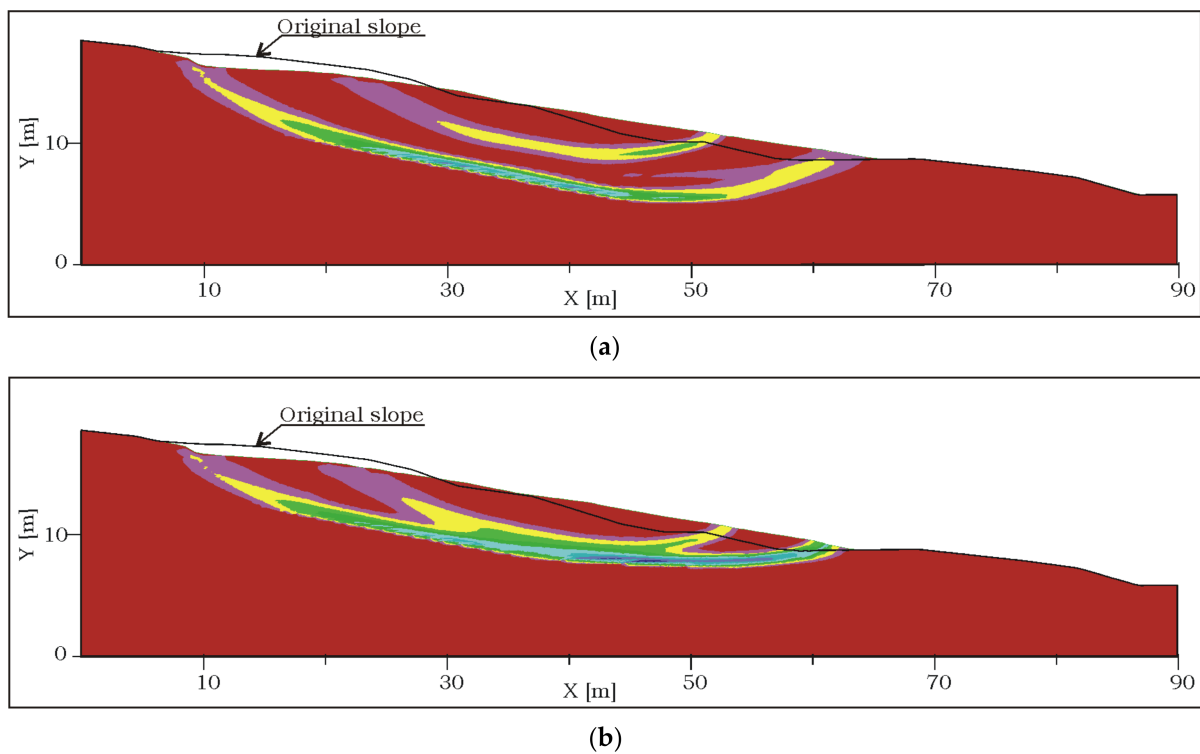


Figure 13. Two slide zones in the upper part of the slope at the time of failure: (a) Model I; (b) Model II.

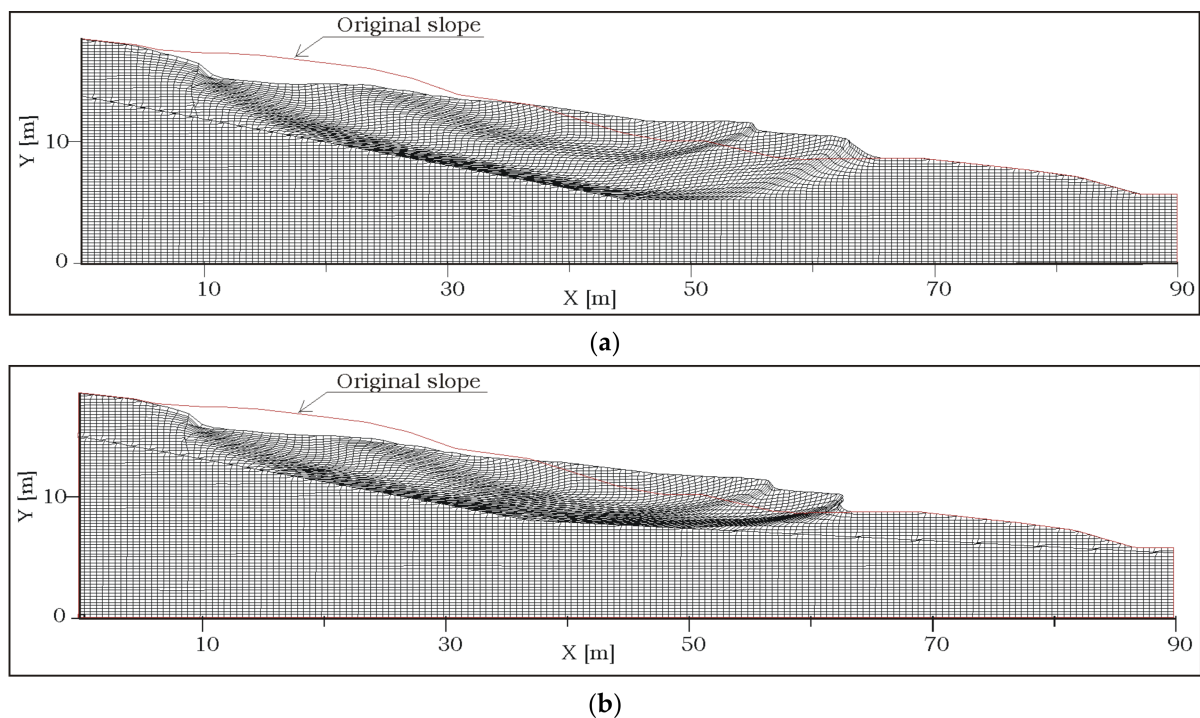


Figure 14. Slope shape at the time of failure according to (a) Model I and (b) Model II.

3.3. Landslide Susceptibility Map of Central Radunia Valley

3.3.1. Relationship between Landslide and Conditioning Factors

The Rutki landslide is one of many landslides in the Central Radunia Valley that have been active since at least the second half of the 19th century (Figure 3b). However, they have not been investigated so far. This study has analysed the relationship between twenty-five conditioning factors and landslide occurrence (Table 2; Figure 15).

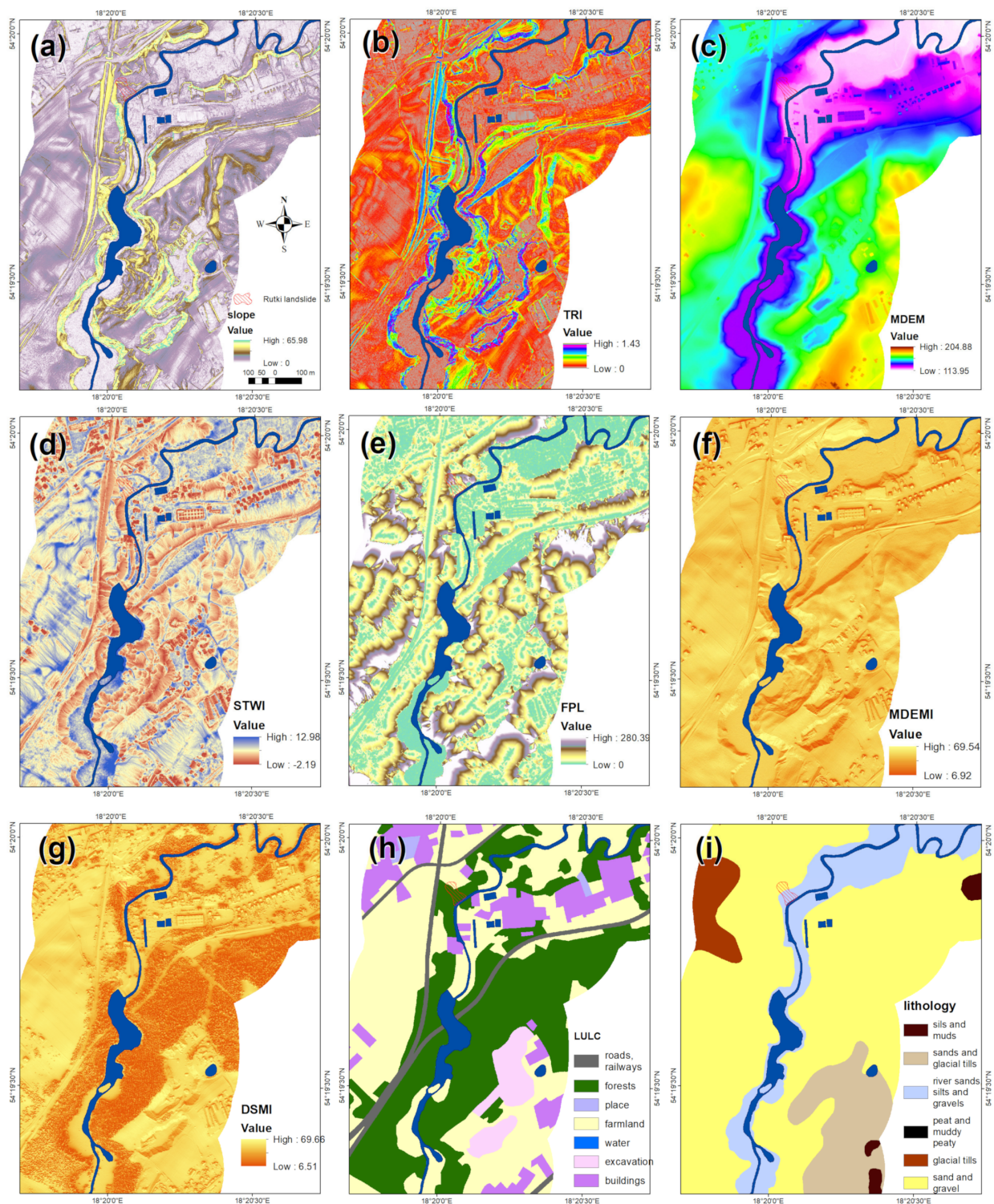


Figure 15. Selected conditioning factors used in GIS analyses. Fragment of study area A (see Figure 1): (a) slope angle; (b) terrain ruggedness index; (c) modified digital elevation model (MDEM); (d) SAGA topographic wetness index; (e) flow path length; (f) MDEM insolation; (g) DSM (modified digital elevation model) insolation; (h) land use and land cover; (i) lithology.

The C&RT method makes it possible to determine the role of individual causal factors. The influence of all the analysed conditioning factors on mass movements in the Radunia Valley as determined using the C&RT method is presented in Figure 16.

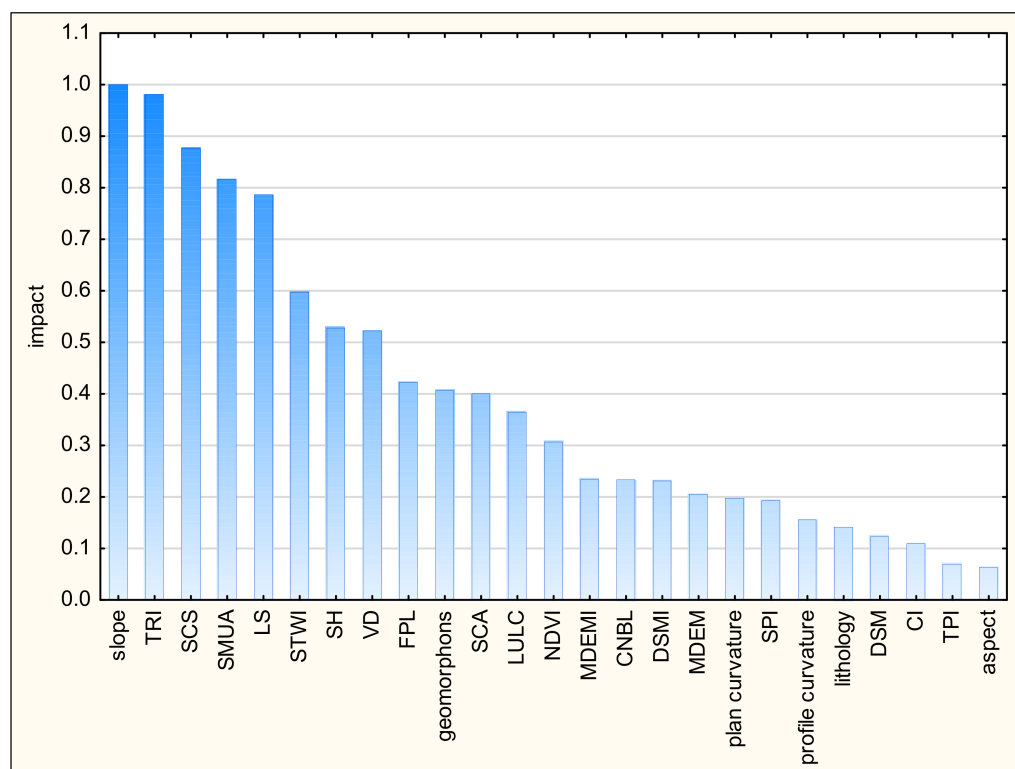


Figure 16. The impact of all the analysed conditioning factors on mass movements in the Central Radunia Valley as determined using the C&RT method. Abbreviations: TRI—terrain ruggedness index, SCS—SAGA catchment slope, SMUA—slope mean of upslope area, LS—length slope factor, STWI—SAGA topographic wetness index, SH—slope height, VD—valley depth, FPL—flow path length, SCA—SAGA catchment area, LULC—land use and land cover, NDVI—normalised difference vegetation index, MDEMI—MDEM insolation, CNBL—channel network base level, DSMI—DSM insolation, MDEM—modified digital elevation model, SPI—stream power index, DSM—digital surface model, CI—convergence index, and TPI—topographic position index.

In the modelling of the landslide susceptibility of the Babi Dół gorge, the most significant geo-environmental variables were the topographic attributes (such as slope angle, TRI, SCS, SMUA, and LS) and the hydrological parameter (STWI) (Figure 16). The results reveal that the slope angle factor is the most influential factor indicating the occurrence of landslides (Figure 16).

The land use and land cover factor ranks 12th (Figure 16), with only the forest class being statistically significant (according to the Wald test, $p < 0.05$).

The interaction between landslide occurrence and LULC is shown on the graph, where the points represent landslide bodies and non-landslide areas used in the GIS analysis (Figure 17). Most of the points representing landslides and that are used in the analysis are located in forested areas (830 points, amounting to 97.99% of all the landslide points used in the analysis). It is noteworthy that lithology (ranked 21st) and aspect (25th) are not significant (Figure 16). A homogeneous geological structure was a minor factor in statistical analysis, but it favours the formation of flows and complex landslides. Most landslides occur in sand and gravel of fluvio-glacial origin (715 points, amounting to 84.42% of all the landslide points used in the analysis) (Figures 15i and 18).

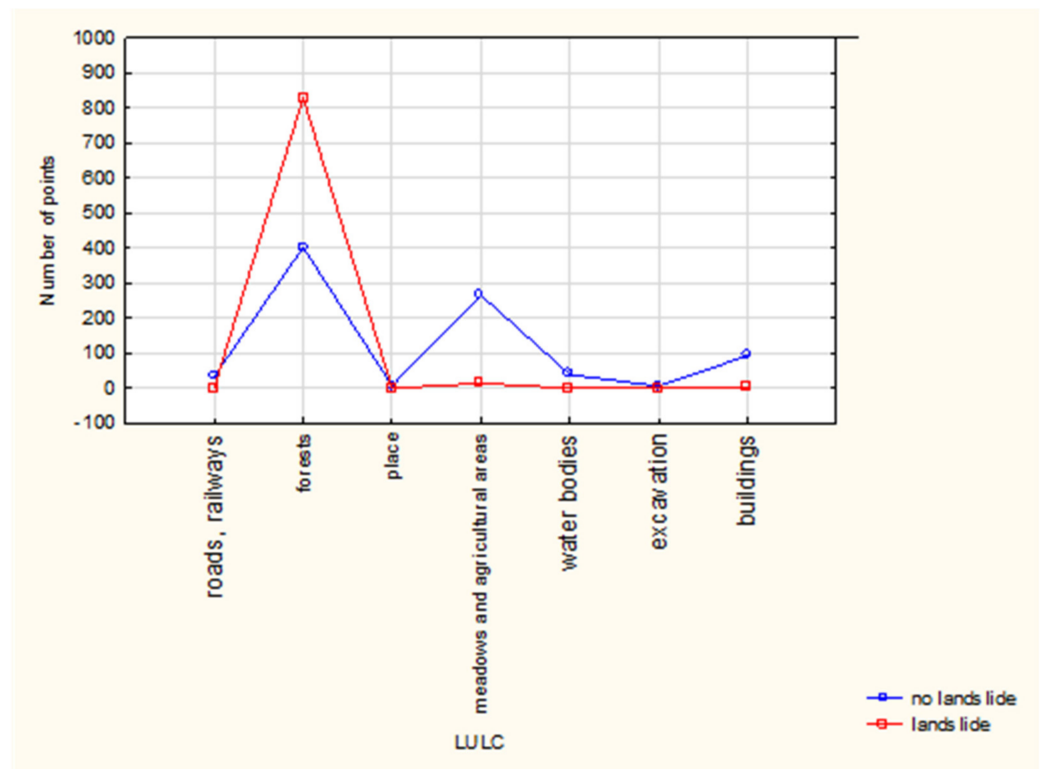


Figure 17. Interdependence between landslide occurrence and LULC. Most of the points representing landslides are located in forested areas.

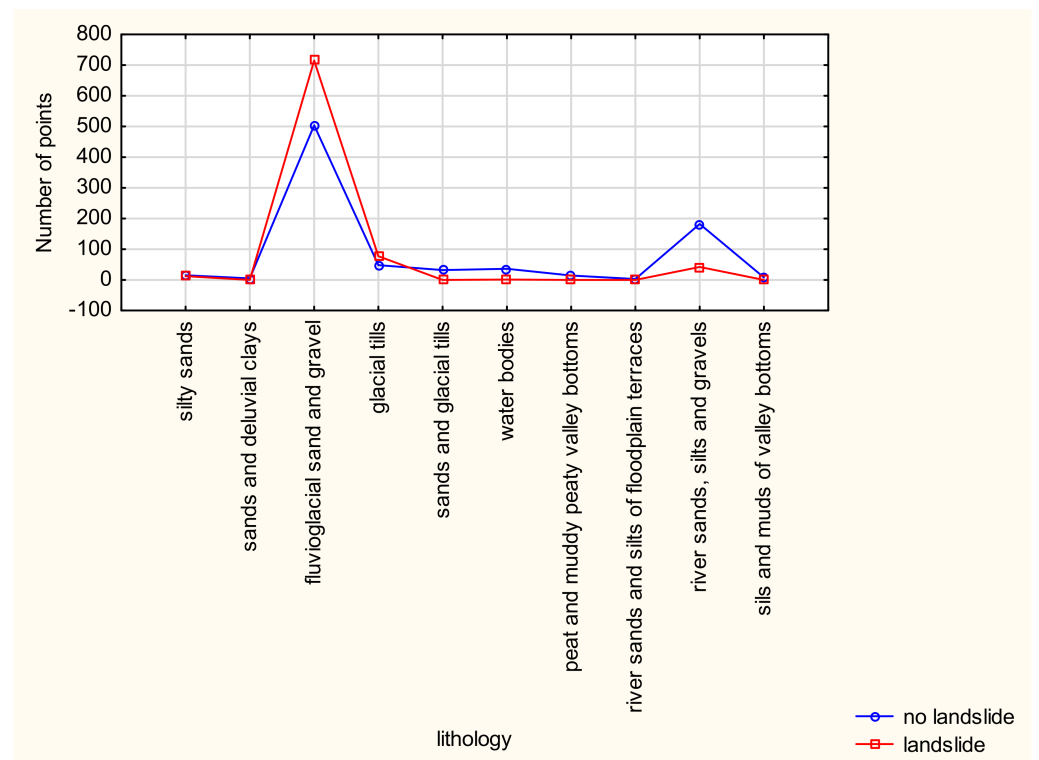


Figure 18. Dependence of landslide occurrence on lithology. Most of the points representing landslides occur in fluvioglacial sand and gravel.

These are also the most common geological sediments in the research area; they occupy 75% of the study area.

Moreover, this result is also confirmed by field studies, as the landslides formed mainly in fluvioglacial sands.

3.3.2. Logistic Regression Model

Landslide susceptibility is determined by considering the interplay between landslide occurrence and the impacts of factors that induce instability. Various combinations of instability factors were used in assessing landslide susceptibility via the LR method.

Different indices have been used to evaluate the performance of a susceptibility model [19]. In this study, to measure the performance of the landslide susceptibility prediction models, their prediction performance was evaluated using model-fitting techniques. The statistical landslide susceptibility models of the Radunia Valley were compared using SRCs and PRCs (Table 4). The SRC and PRC curves for the two chosen models are shown in Figure 19.

Table 4. Ranking of the model configurations according to their effectiveness.

| Model | AUC for SRC (%) | AUC for PRC (%) |
|---------|-----------------|-----------------|
| Model 1 | 94.52 | 93.65 |
| Model 2 | 87.84 | 85.34 |
| Model 3 | 91.80 | 87.33 |
| Model 4 | 89.25 | 87.87 |

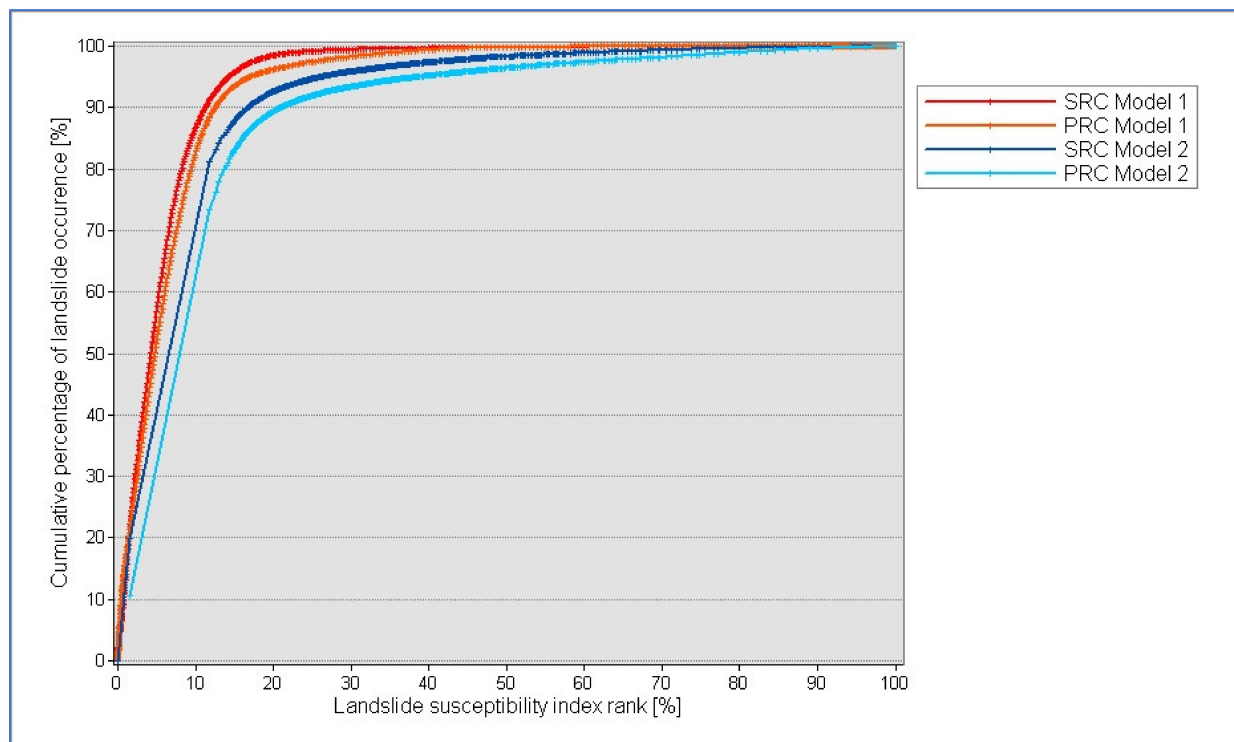


Figure 19. Prediction and success rate curves for two chosen models. Abbreviations: SRC—success rate curve; PRC—prediction rate curve.

In the first stage of susceptibility modelling, all 25 conditioning factors (Table 2, Figure 15) were used. For Model 1, the SRC AUC value = 94.52%, and the PRC AUC value = 93.65% (Figure 19, Table 4). The AUC values > 90% are typical of a model with excellent ability [78].

In the LSM modelling of the Central Radunia Valley using LR, the most significant geo-environmental variable was slope (Figure 16). Therefore, in Model 2, only the strongest

factor, i.e., the slope, was taken into account. For Model 2, the SRC AUC value = 87.84%, and the PRC AUC value = 85.34% (Figure 19, Table 4). A model is considered reliable if its AUC values are higher than 70% [78].

Model 3 uses only variables that are significant (according to the Wald test, $p < 0.05$) and not overly correlated with each other. The choice of predictive variables (factors) was carried out by forward stepwise approach. This model does not take into account qualitative variables. In order to determine the collinearity of the variables, i.e., the grouping of predictors in terms of similar features, PCA was performed (Table 5).

Table 5. Results of principal component analysis (PCA). The table shows values of the scores obtained for each independent variable for each factor. Abbreviations: vide Figure 16 or Table 2.

| Original Variable/Conditioning Factors | Factor Loadings (Varimax Normalised) Extract: Principal Components (the Marked Loadings Are > 0.7) | | | | |
|----------------------------------------|----------------------------------------------------------------------------------------------------|-------------|-------------|-------------|-------------|
| | Component 1 | Component 2 | Component 3 | Component 4 | Component 5 |
| TRI | 0.88 * | −0.05 | 0.16 | 0.30 | −0.09 |
| SMUA | 0.87 | −0.12 | −0.15 | 0.14 | −0.04 |
| VD | 0.47 | −0.14 | −0.37 | 0.67 | −0.06 |
| TPI | −0.08 | 0.33 | 0.77 | −0.32 | 0.01 |
| LS | 0.40 | −0.03 | 0.28 | 0.54 | −0.16 |
| CI | −0.01 | 0.00 | 0.10 | 0.01 | 0.71 |
| profile curvature | −0.13 | 0.06 | 0.68 | −0.15 | 0.29 |
| plan curvature | 0.04 | −0.04 | 0.07 | −0.18 | 0.79 |
| slope | 0.89 | −0.05 | 0.16 | 0.31 | −0.09 |
| SH | 0.58 | 0.16 | 0.64 | 0.13 | 0.06 |
| NDVI | 0.47 | 0.19 | −0.16 | 0.17 | 0.11 |
| CNBL | −0.07 | 0.97 | −0.02 | 0.00 | 0.02 |
| SCA | −0.01 | 0.02 | −0.06 | 0.80 | −0.09 |
| SCS | 0.89 | −0.15 | −0.10 | 0.20 | −0.08 |
| STWI | −0.87 | 0.04 | −0.15 | 0.16 | −0.06 |
| FPL | 0.32 | −0.02 | −0.17 | 0.69 | 0.04 |
| SPI | 0.12 | 0.02 | 0.56 | 0.46 | −0.28 |
| MDEMI | −0.25 | 0.10 | −0.11 | 0.02 | 0.26 |
| DSMI | −0.56 | −0.28 | 0.12 | −0.11 | 0.07 |
| MDEM | −0.07 | 0.95 | 0.20 | −0.06 | 0.01 |
| DSM | 0.09 | 0.95 | 0.19 | −0.02 | 0.01 |

* The red values show the results for conditioning factors (variables) correlated with each other in individual groups.

As a result of the findings yielded by Model 3, seven conditioning factors were taken into account, i.e., slope, VD, SH, MDEMI, TPI, NDVI, and MDEM. For Model 3, the SRC AUC value = 91.80%, and the PRC AUC value = 87.33% (Table 4).

In the next stage of susceptibility modelling, only the best eight conditioning factors, i.e., slope, TRI, SCS, SMUA, LS, STWI, SH, and VD, were used. For Model 4, the SRC AUC value = 89.25%, and the PRC AUC value = 87.87% (Table 4).

The results of the subsequent LR modelling are not included in this paper as they yielded intermediate results with respect to Models 1 and 2. None of the models that took into account different variables (e.g., independent variables, variables not overly correlated) after verification were better than Model 1.

The final landslide susceptibility maps of the Central Radunia Valley (with a scale of 1:5000) created using calculations obtained via the LR technique and different sets of instability factors are presented in Figure 20. The first map was created using all 25 conditioning factors (Model 1) whereas only the slope (Model 2) was taken into account in the second map.

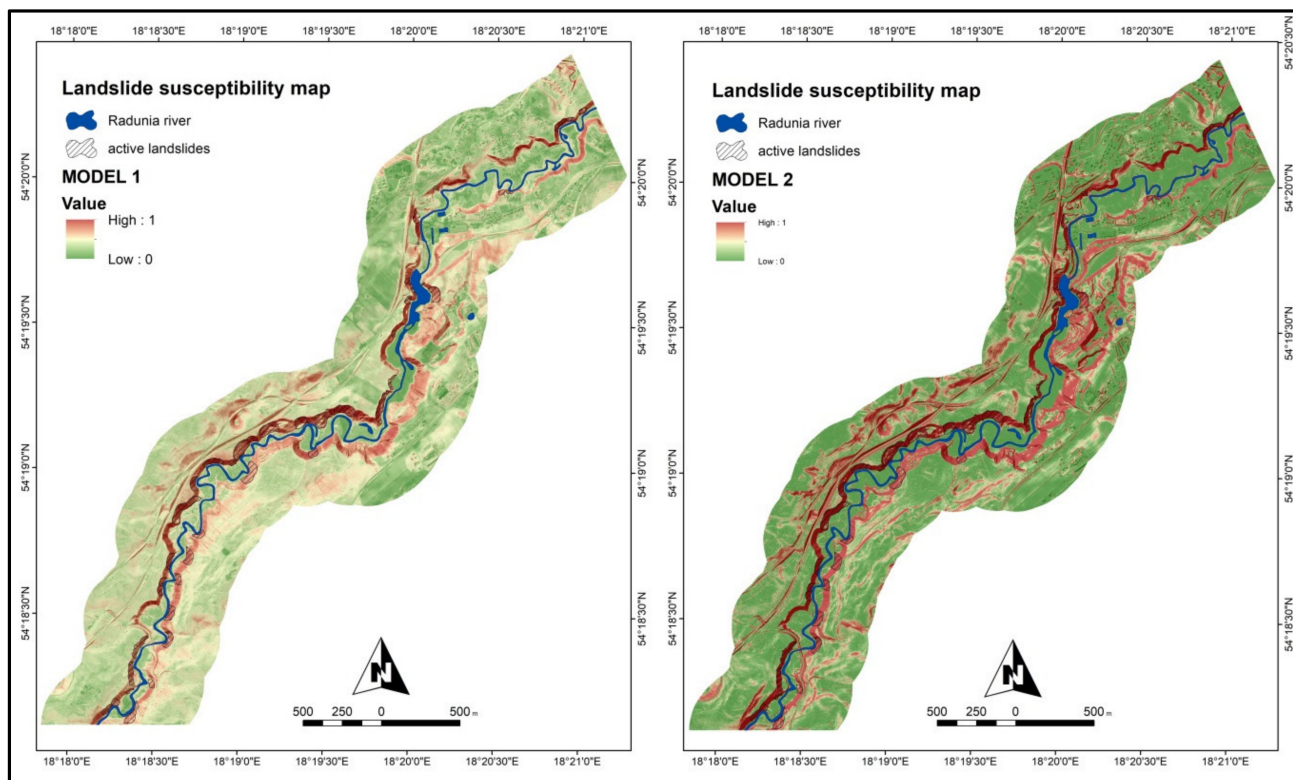


Figure 20. Landslide susceptibility mapping of the Central Radunia Valley using a geographic-information-system-based statistical model (logistic regression method). Model 1—developed using all 25 conditioning factors; Model 2—developed using only the strongest factor, i.e., slope.

Model 2, due to the fact that only the slope was considered highly susceptible includes many infrastructure elements (roads, railroads), where mainly sheet and rill erosion can occur. On the other hand, Model 1 was created by considering the interactions of a greater number of factors; thus, it provides a more realistic picture of landslide susceptibility.

4. Discussion

Susceptibility prediction models help to forecast the future processes in a study area. Numerical modelling based on the geomechanical approach, on the other hand, makes it possible to determine the mechanism of a landslide's formation, its causes, and the depth of the slide zones. Cross-disciplinary studies complement each other and allow for a deeper recognition of the causes and mechanisms of landslide formation. To date, however, such comprehensive studies have rarely been undertaken [79]. There has also been no discussion of the usefulness of other methods (e.g., numerical analyses, geological analyses) in verifying the role of conditioning factors calculated using statistical methods.

4.1. Landslide-Triggering Factors

Landslides in the Central Radunia Valley can be triggered by natural physical processes such as the undercutting of a slope on the outer side of a river meander and heavy rainfall. Moreover, landslide activation and deactivation are a combination of natural and anthropogenic processes. Precipitation > 100 mm/day can trigger landslides in the study area. These amounts of rainfall have activated landslides in Gdańsk and Gdynia (about

30 km from Rutki) [80]. According to Starkel [81], short-lasting downpours with a small spatial extent, amounting to 20–150 mm, and with a high minute intensity (approximately 2–4 mm/min) initiate the formation of flows. Due to the area's geological structure, i.e., the presence of sands and gravel of fluvioglacial origin (they occupy 75% of the study area), earthflows in the Radunia Valley are a common type of mass movement. A landslide of this type occurred in 1980 in the area of today's kayak mooring in Borkowo. In 1980, there was intense (higher than average) rainfall, totalling 868 mm/year [30,31]. Landslides in the northern part of the Central Radunia Valley can also be generated by human activities such as slope excavation and land cover changes redirecting rainfall runoff in such a way that the flow is concentrated (Figure 2b,c) [82]. In the northern part of the study area, human activity has a large impact on the formation, activation, and reactivation of landslides.

In 2019, the Rutki landslide was reactivated during the horizontal drilling of a borehole. As regards the site, the initiating nature of horizontal drilling was indicated, which, so far, has not been considered an anthropogenic triggering factor influencing the formation of landslides. Triggering factors such as intense precipitation, volcanic eruptions, and earthquakes have often been discussed in the literature [83,84]. Anthropogenic factors, which include undercutting, slope gradient changes, ill-considered logging, fire-removed vegetation, reductions in infiltration and retention areas, and uncontrolled runoff along road surfaces, are frequently referred to in the literature [20,80,85–87]. A landslide that formed during seismic profiling in the vicinity of Lake Brzeźno (northern Poland) was also noted [88,89]. According to an experienced driller, drilling-activated landslides might have occurred as well. In the case of Rutki, it is hypothesised that vibrations and the pumping of water into the borehole led to the weakening of the sand and its transition into sandwater flow. This could have caused the disruption of the continuity of natural underground waterways. The route of the horizontal drilling and the change in the location of the springs (after activating the landslide; Figures 4 and 5) indicate that the borehole was drilled into the aquifer. This resulted in a change in the outflow of groundwater. Hypothetically, this might have caused the fusion of aquifers that were not in hydraulic contact or the fusion of privileged groundwater flow paths. It also seems that the confined groundwater zone plays a role in controlling slope failure in Rutki. According to Jiao et al. [90], a confined groundwater flow regime, in connection with triggering factors, results in a significant reduction in slope stability.

New ponds and springs formed on the slide after the failure (Figure 2e, Figure 4, and Figure 6), indicating the retention of water (creating a kind of underground water reservoir under temporary pressure) and its sudden relaxation as a consequence of the fast opening of the waterways for unrestrained flow down the slope. According to Montgomery and Dietrich [91], channel initiation is influenced by landsliding. Periodic, small-scale, shallow landslides on steep slopes can create a topographic depth where subsurface flow can begin to exfiltrate [91].

The process of boring resulted in the groundwater outflow change, or the water was retained as the underground outflow was blocked by the bentonite. The drillers used bentonite to stabilise the borehole walls. Swelling bentonite forms a highly impermeable barrier [92] that might have blocked the flow of groundwater, and its rapid release might have activated the landslide. The close proximity of the railway line and the road is also significant for this landslide. Vibrations caused by traffic have a negative impact on the stability of non-cohesive soils.

4.2. The Role of Causal Factors in the Formation of Landslides

Susceptibility prediction models play an important role in establishing the relationship between landslides and their causal factors. In the current study, the best susceptibility model was obtained using a large number of causal factors, i.e., 25, which suggests that many different factors influence susceptibility in lowlands (young morainic areas). This is confirmed by the results of previous susceptibility assessments in lowland areas: Gdańsk and Gdynia [20,69] and the Lower Vistula Valley [93].

Current studies indicate that not all important and identifiable factors can be included in susceptibility assessment. One of the most important factors is hydrogeological conditions. The reconstruction of the Rutki landslide using geological cross-sections and numerical methods confirms the great importance of groundwater level conditions. A lack of a sufficient number of boreholes, poor hydrogeological reconnaissance, and the diversified and time-variable location of the first aquifer made it impossible to compile an accurate hydrogeological map that could be included in the GIS analysis. The importance of hydrogeological conditions is also indicated by field observations and the groundwater level measurements taken by piezometers. In this context, the description of the role of causal factors purely based on GIS layers [94–96] might sometimes seem ambiguous.

Moreover, in the analysed area, the first aquifer has a dynamic character. Changes in the location of groundwater flow paths connected with the rising or lowering of the groundwater table (also resulting from changes in surface water conditions) and changes in the locations of springs may play an important role. Anthropogenic activities also contribute to this state, which was evident when comparing the results of archival geotechnical documentation with the current results of field surveys (Figures 4 and 5). The changeability of hydrological conditions is also evident in past and present maps. For example, the former watercourse in the Borkowo area, marked on the Messtischblatt map from 1900 [53], is currently dry and partly built-up (railway embankment and a culvert) (Figures 3 and 7c). However, in the anthropogenically unchanged part, STWI and FPL reflect the former water flow paths (Figure 15d,e).

Geological structure is always included in GIS analyses and is usually relevant [61,65,93]. In the susceptibility analysis of the Central Radunia Valley, the area's geological structure was deemed insignificant. This is due to the fact that the study area is dominated by sands. However, boreholes reveal a more compound glacial stratigraphic architecture (Figure 5). In young glacial areas, complex geological layering (the presence of low-strength data) has the greatest influence on landslides [93]. The position and thickness of low-strength strata act as a first-order control factor affecting landslide volume and groundwater flow [97]. In the Rutki landslide, complex geological layering also has an impact on hydrological conditions (Figure 5).

In the case of the Central Radunia Valley, there is a lack of data on the area's deep geological structure due to the small amount of drilling conducted in the region. Moreover, field surveys have shown the influence of the surface geological structure on the type of landslide that occurs (slides and flow). Sands are highly sensitive to water, and only a small increase in water content would be enough to liquefy this material. This type of geological structure (with a predominance of sand) and shallow groundwater levels have an impact both on the large number of shallow landslides occurring here and the mechanisms of their formation. Subsequently, sands are less resistant to rill and gully erosion [98]. In the Rutki landslide, in the past as well as now, mass movement and impermanent gully erosion have overlapped (Figures 3c and 4). This result was further confirmed via GIS analysis. The significant impact of STWI and FPL on mass movement in the Central Radunia Valley (Figures 15 and 16) reveals that flows, rill, and gully erosion can play a significant role in a study area. The high STWI value also corresponds with the gully erosion observed after landslide reactivation in 2019 (Figures 4, 7d and 15d). According to Persichillo et al. [99], the investigation of the most important predisposing factors could lead to the broadening of the knowledge about the mechanisms regulating landslide occurrence.

An important problem in susceptibility mapping consists of the interrelationships between conditioning factors [100,101]. Multicollinearity arises when at least two highly correlated predictors are assessed simultaneously in a regression model. In the case of the Central Radunia Valley, many factors calculated using DEM are correlated, as clearly shown in the correlation and PCA analyses (Table 5). However, the inclusion of different sets of independent data in the model did not allow for the optimisation of the model. In the Radunia Valley, shallow rain-induced landslides occur. The slip surface depth usually does not exceed 2–4 m, and the shape of this surface corresponds to the ground

surface. Such landslides are mostly influenced by the geometry of slopes. Therefore, the phenomena and processes occurring on the ground surface can significantly influence landslide susceptibility. Topographic attributes are frequently used as surrogates of physical processes [102]. Some of them have a significant influence on the activation of shallow landslides. The most important of these attributes include surface runoff, fluvial erosion, and solar input (Figure 15d–g). Current research suggests that including correlated data in LR models can even improve prediction performance. However, in cases where it is vital to accurately explain the role played by the variables entered into the model [103,104], introducing only independent variables into the LR prediction model is justified. Moreover, multicollinearity in logistic regression does not adversely affect the overall fit or predictions of a model [104]. In the susceptibility assessment of the Central Radunia Valley, very important factors (i.e., the role of groundwater and complex geological layering) have been omitted in the analysis. The great importance of these two factors for young glacial areas has been shown in previous studies [20,93]. Including STWI, which indicates the spatial distribution and extent of saturation areas [102], improves prediction results. Another important element is insolation (DSMI and MDEMI in Figure 15f,g), which affects humidity and evaporation. This can be explained by the fact that in the LR method, omitting an important factor in the model specification process can worsen the results [70].

4.3. The Roles of High-Resolution DEMs and Modified DEMs in Susceptibility Assessment

Currently, an important tool for use in landslide studies is a high-resolution DEM [56,105–107]. LiDAR or laser scanning can provide high-resolution topographic information [13]. Topographic attributes developed using a DEM play an important role in the modelling of landslide formation as they depict various geomorphological and hydro-geological processes. The usefulness of topographic attributes in susceptibility analyses has been highlighted by various authors [19,20,59,69,87,95,96,108]. Susceptibility assessments are conducted on a global, European, national, and local scale [93,109,110,110,111]. Westen et al. [112] distinguished medium from large and detailed scales of susceptibility assessment analysis. The selection of the scale of analysis is usually determined by the intended application of the mapping result [113]. Additionally, the analysis scale has a substantial influence on the results of the model in question [114]. Grabowski et al. [91] argued that a small scale does not always produce correct results. For local spatial scale studies, more accurate predisposing factors (in terms of map scale or spatial resolution) should be used [72]. According to Polykretis et al. [114], spatial resolution constitutes a key factor in the accuracy of an LS assessment, and the optimal size of grid cells depends on the size of the study area. However, it is worth noting that DEMs used for modelling susceptibility with small scales are highly generalised. Resolution (ranging from a maximum of 1 m to a minimum of 100 m) has a significant impact on the accuracy of digital elevation models [115]. The most serious errors affect slope angle; therefore, models with the highest possible resolution, no less than 10 m, should be used [115]. Slope is the most influential and essential parameter of landslide susceptibility; thus, a high-resolution DEM is crucial. According to Polykretis et al. [114], a detailed scale analysis is more appropriate for landslide susceptibility assessment in the Northern Peloponnese (Greece). Equally, the use of a regional scale in a river valley entrenched in a lowland plateau is better, as it allows for the preparation of a susceptibility map taking into account the local specificity [93]. Landslide susceptibility mapping with large and detailed scales has been carried out on several successful occasions. Zêzere et al. [72] made landslide susceptibility maps of the Silveira Basin (18.2 km²), for which a pixel size of 5 × 5 m was adopted. Persichillo et al. [99] made landslide susceptibility maps of the Rio Fate study area, which has a surface area of 1.9 km², and the Vernazza study area, which has a surface area of 5.7 km². The resolution (pixel size) of the input data used in the analysis conducted by Persichillo et al. [99] was 10 × 10 m. According to Persichillo et al. [99], a 10 × 10 m spatial resolution of input data is not very useful when taking into account all detailed terrain information and likely has a negative influence on the results. In the current study, a small area of the Radunia

Valley (4.75 km²) was selected, and a detailed raster cell size of 1 × 1 m was used. The high-resolution DEM based on the LIDAR data used in our modelling approach allowed for high spatial resolution of topographic attributes and might have contributed to the very high values (AUC > 90%) of the SRC and PRC curves.

Furthermore, in this study, a DEM has been modified by adding buildings (MDEM). So far, DEMs revealing the surface of land without taking into account building infrastructure have been used. It would be advisable to use both of these models (a DEM and the MDEM) at the same time, as they are differently suitable for calculating topographic attributes (Figure 13). According to our research, it is better to calculate slopes based on a DEM (Figure 13). In the MDEM, slopes are also calculated for buildings, which may result in an overestimation of susceptibility for flat built-up areas. In contrast, the MDEM is particularly useful for calculating STWI and FPL, as it indicates changes in rainwater runoff associated with the infrastructure of buildings (Figure 15d,e). This is crucial in environments that are changing dynamically. Buildings increase the amount of impervious land cover, thereby reducing infiltration and increasing surface runoff [116,117].

The Radunia Valley susceptibility maps show some differences in the frequency of landslides in the northern and southern parts of the study area. In the northern part, there are fewer landslides due to significant anthropogenic changes, which include a large number of drains and other forms of engineering protection. However, landslide susceptibility in these areas is analogous (Figure 20). Furthermore, the maps show some differences between the left and right banks of the Radunia River. The left bank is characterised by much higher susceptibility. Additionally, the railway lines located on this side of the river are at risk (Figure 1), as some of the main slopes of active landslides are situated within several metres from the railway embankment. It should be noted that there are higher STWI values on the left side of the river along the railway embankment (Figure 15d). The accumulation of surface water on the western side along the left side of the embankment and the presence of landslides associated with the river valley on the right side of the embankment may pose a major threat to the railway line in the future. This is also important in the context of its planned expansion. On the other hand, in the northern part of the study area, new houses and housing estates have been built in the immediate vicinity of the Radunia Valley over the last few years. This new development produces additional loads, results in changes in landform, and impedes the infiltration of rainwater. These factors indicate a high risk for the northern section of the Radunia Valley; therefore, possible changes in land use planning should be considered.

5. Conclusions

This study attempted to analyse the mechanisms and factors contributing to shallow soil landslides in river valleys entrenched in lowlands based on the example of the Central Radunia Valley. The combination of the susceptibility analysis, field studies, and geomechanical modelling of the Rutki landslide clearly demonstrates the benefits of cross-disciplinary studies, which lead to the improvement of knowledge about landslides' causal and triggering factors and landslide mechanisms. The aesthetic value and diversity of nature of the river valleys in the lowland areas of northern Poland make these areas attractive and likely to be sold for development. An assessment of landslide susceptibility in these areas is therefore particularly important for landslide risk reduction.

In this study, landslide susceptibility for the Central Radunia Valley was calculated using the LR method. It was determined that the most significant causal factor that affects the likelihood of a landslide is connected with geomorphological conditions. According to the results acquired using the C&RT method, the impact of individual topographic attributes, such as slope, TRI, SCS, SMUA, LS, SH, and VD, is greater than 0.5, while geological structure is one of the least important of the significant factors and its impact is less than 0.2 (21st place; Figure 16). This is because the area is dominated by sands and gravel of fluvioglacial origin (they occupy 75% of the study area). Almost 85% of landslides occur within these common geological sediments. The lack of the lithological

differentiation of the soil reduces the statistical significance of this factor. The current study also showed that the greatest influence on landslide formation is the slope, and this one factor developed using a high-resolution DEM is sufficient to produce a reliable map (SRC AUC value = 87.84%; PRC AUC value = 85.34%). These results indicate that a preliminary susceptibility map can easily be developed for young morainic areas.

The Rutki landslide has existed since at least the second half of the 19th century and its formation and activation is linked to river erosion on the outer side of the meander (Figure 3b). From at least the beginning of the 20th century, the mass movements have been accompanied by linear erosion (gullies) above the main scarp (Figure 3c). The landslide was reactivated in January 2019. The description of the landslide process, confirmed mainly using advanced numerical simulations, clearly indicates the influence of the drilling of a horizontal borehole in the area of the future main landslide scarp (Figures 4 and 7a). The water used while drilling hydrated the soil and thus weakened its stability. After the landslide formed above the main scarp, a gully (10 m long) was formed, causing growing of the landslide in the direction opposite to its own motion (Figure 4). The movement (rotational slide) begun in the upper part of the landslide (source area) and was continued by flow in the lower part (accumulation zone) (Figure 8). The numerical modelling conducted in this study indicates the presence of two slip zones that are 1–2 m thick. For Model I, two separate slip zones were visualised at depths of 2–3 and 5–6 m b.g.l (Figure 13a). In contrast, Model II showed two slip surfaces in contact with each other in the central part at depths of 2–3 and 3–5 m b.g.l (Figure 13b). The first slide zone (Models I, II) is approximately in alignment with the location of the silt layer. The landslide was partially stabilised in the spring of 2020, resulting in a lowering of the groundwater table (about 0.5). Since then, within the unprotected older part of the landslide, there has been downhill creep to a depth of 2 m, with a velocity of 0.5 mm/month (Figure 10a,b). Groundwater occurs here at a depth of approximately 3 m.

The numerical modelling and geological recognition of the investigated landslide's cross-section additionally reveal a significant role of complex geological layering and the groundwater level (Figures 5 and 12). It is important to note that in the study area, not all relationships between the conditioning factors and landslides can be represented using GIS-based statistical models. Limitations arise due to the lack of data and the dynamic, changeable characters of the processes that occur in anthropogenically changed areas. In the Central Radunia Valley, hydrological conditions in connection with the area's geological structure also have a major influence on the type and mechanism of mass movements (slide-flow).

Author Contributions: Conceptualisation, A.M, L.Z., F.E. and A.K.; methodology, A.M, L.Z, F.E. and A.K.; software, A.M., L.Z. and F.E.; validation, A.M. and L.Z.; formal analysis, A.M., L.Z. and F.E.; investigation, A.M. and L.Z.; resources, A.M.; data curation, A.M.; writing—original draft preparation, A.M., L.Z.; writing—review and editing, A.M., L.Z., A.K. and F.E; visualisation, A.M, L.Z. and F.E.; supervision, A.M; project administration, A.M; funding acquisition, A.M. All authors have read and agreed to the published version of the manuscript.

Funding: This research project was partly funded by the Polish Geological Institute, National Research Institute (Grant No. 62.9012.1950.00.0 and Grant No. 61.3506.2001.00.0) and partly by National Science Centre, Poland (Grand No. 2020/04/X/ST10/00575).

Data Availability Statement: Data are available in a publicly accessible repository. Additional maps and photos are available at <https://www.pgi.gov.pl/gdansk/projekty-krajowe/osuwiska-doliny-raduni.html> (accessed on 10 January 2023). The data presented in this study are also available in ZENODO at <https://doi.org/10.5281/zenodo.6907702> (accessed on 10 August 2022).

Acknowledgments: The authors thank the anonymous reviewers for their accurate comments and suggestions, which have greatly improved the quality of the manuscript. The authors are grateful to Mirosław Błaszkiwicz, and Mirosław Lidzbarski, and Grzegorz Migut, for their valuable ideas. The authors would like to thank Energa S.A. Group, Poland, for the free access to the observation of water levels in the Radunia River and precipitation data. The authors would also like to thank Adam Trubłajewicz for his help with translation and proofreading.

Conflicts of Interest: The authors declare no conflict of interest.

References

1. Ostoja-Zagórski, J. *Najstarsze Dzieje Ziemi Polskiej*; Wydawnictwo Uniwersytetu Kazimierza Wielkiego w Bydgoszczy: Bydgoszcz, Poland, 2005; p. 252.
2. Thiel, K. *Kształtowanie Fliszowych Stoków Karpackich Przez Ruchy Masowe—Na Przykładzie Badań Na Stoku Bystrzyca w Szymbarku*; Prace Instytutu Budownictwa Wodnego PAN: Gdańsk/Kraków, Poland, 1989; Volume 17, p. 91.
3. Gil, E. Meteorological and hydrological conditions of landslides, Polish Flysch Carpathians. *Stud. Geomorphol. Carpatho-Balc.* **1997**, *31*, 143–158.
4. Glade, T. Modelling landslide triggering rainfall thresholds at a range of complexities—Landslides in Research, Theory and Practice. In Proceedings of the 8th International Symposium on Landslides, Cardiff, UK, 26–30 June 2000; Bromhead, E., Ed.; pp. 633–640.
5. Gil, E.; Zabuski, L.; Mrozek, T. Hydrometeorological conditions and their relation to landslide processes in the Polish Flysch Carpathians (an example of Szymbark area). *Stud. Geomorphol. Carpatho-Balc.* **2009**, *43*, 127–143.
6. Tyszkowski, S. Badania rozwoju osuwisk w rejonie Świecia, na podstawie materiałów fotogrametrycznych. *Landf. Anal.* **2008**, *9*, 385–389. (In Polish)
7. Tyszkowski, S. Distribution and origin of contemporary lowland landslides in the area of the direct river impact, on the example of section of Lower Vistula Valley between Morsk and Wiąg. *Landf. Anal.* **2014**, *25*, 159–167, (In Polish with English Summary). [[CrossRef](#)]
8. Lévy, S.; Jaboyedoff, M.; Locat, J.; Demers, D. Erosion and channel change as factors of landslides and valley formation in Champlain Sea Clays: The Chacoura River, Quebec, Canada. *Geomorphology* **2012**, *145–146*, 12–18. [[CrossRef](#)]
9. Yenes, M.; Monterrubio, S.; Nespereira, J.; Santos, G.; Fernández-Macarro, B. Large landslides induced by fluvial incision in the Cenozoic Duero Basin (Spain). *Geomorphology* **2015**, *246*, 263–276. [[CrossRef](#)]
10. Kaczmarek, H.; Tyszkowski, S.; Banach, M. Landslide development at the shores of a dam reservoir (Włocławek, Poland), based on 40 years of research. *Environ. Earth Sci.* **2015**, *74*, 4247–4259. [[CrossRef](#)]
11. Korup, O. Landslide dam. In *Encyclopedia of Geomorphology*; Goudie, A., Ed.; Routledge: London, UK, 2004; 1156p.
12. Korup, O. Large landslides and their effect on sediment flux in South Westland, New Zealand. *Earth Surf. Process. Landf.* **2005**, *30*, 305–323. [[CrossRef](#)]
13. Glenn, N.F.; Streutker, D.R.; Chadwick, D.J.; Thackray, G.D.; Dorsch, S.J. Analysis of LiDAR-derived topographic information for characterizing and differentiating land-slide morphology and activity. *Geomorphology* **2006**, *73*, 131–148. [[CrossRef](#)]
14. Fuller, I.C.; Riedler, R.A.; Bell, R.; Marden, M.; Glade, T. Landslide-driven erosion and slope–channel coupling in steep, forested terrain, Ruahine Ranges, New Zealand, 1946–2011. *Catena* **2016**, *142*, 252–268. [[CrossRef](#)]
15. Alonso, E.E.; Pinyol, N.M.; Puzrin, A.M. *Catastrophic Slide: Vaiont Landslide, Italy*; Alonso, E.E., Pinyol, N.M., Puzrin, A.M., Eds.; Geomechanics of Failures; Advanced Topics; Springer: Dordrecht, The Netherlands; Heidelberg, Germany; London, UK; New York, NY, USA, 2010; pp. 33–81.
16. Wolter, A.; Stead, D.; Ward, B.C.; Clague, J.J.; Ghirotti, M. Engineering geomorphological characterisation of the Vajont Slide, Italy, and a new interpretation of the chronology and evolution of the landslide. *Landslides* **2015**, *13*, 1067–1081. [[CrossRef](#)]
17. Guzzetti, F.; Reichenbach, P.; Cardinali, M.; Galli, M.; Ardizzone, F. Probabilistic landslide hazard assessment at the basin scale. *Geomorphology* **2005**, *72*, 272–299. [[CrossRef](#)]
18. Pourghasemi, H.R.; Pradhan, B.; Gokceoglu, C.; Mohammadi, M.; Moradi, H.R. Application of weights-of-evidence and certainty factor models and their comparison in landslide susceptibility mapping at Haraz watershed, Iran. *Arab. J. Geosci.* **2013**, *6*, 2351–2365. [[CrossRef](#)]
19. Reichenbach, P.; Rossi, M.; Malamud, B.; Mihir, M.; Guzzetti, F. A review of statistically-based landslide susceptibility models. *Earth-Sci. Rev.* **2018**, *180*, 60–91. [[CrossRef](#)]
20. Małka, A. Landslide susceptibility mapping of Gdynia using geographic information system-based statistical models. *Nat. Hazards* **2021**, *107*, 639–674. [[CrossRef](#)]
21. Banach, M.; Kaczmarek, H.; Tyszkowski, S. Development of landslides in shore zones of water reservoir on an example of the central landslide at Dobrzyń on the Vistula, Włocławek Reservoir. *Przegląd Geogr.* **2013**, *85*, 397–415. (In Polish) [[CrossRef](#)]
22. Bernardie, S.; Desramaut, N.; Malet, J.-P.; Gourlay, M.; Grandjean, G. Prediction of changes in landslide rates induced by rainfall. *Landslides* **2015**, *12*, 481–494. [[CrossRef](#)]
23. Vassallo, R.; Grimaldi, G.M.; Di Malo, C. Pore pressures induced by historical rain series in a clay landslide: 3D modelling. *Landslides* **2015**, *12*, 731–744. [[CrossRef](#)]

24. Zabuski, L.; Kulczykowski, M. Współczesne procesy osuwiskowe na klifie w Jastrzębiej Górze. *Przegląd Geol.* **2020**, *68*, 682–690. Available online: <https://www.pgi.gov.pl> (accessed on 8 January 2022).
25. Zabuski, L.; Kulczykowski, M.; Świdziński, W. Identification of the Causes of a Landslide in Koronowo (Polish Lowlands). *AHEM* **2019**, *66*, 47–56. [[CrossRef](#)]
26. Marks, L. Timing of the late Vistulian (wechselian) glacial phases in Poland. *Quat. Sci. Rev.* **2012**, *44*, 81–88. [[CrossRef](#)]
27. Rachocki, T. Przebieg i natężenie współczesnych procesów rzecznych w korycie Raduni. *Dok. Geogr.* **1974**, *4*, 7–121.
28. Piasecki, D. Szkic geologiczno-morfologiczny dorzecza Raduni. *Rocz. Pol. Tow. Geol.* **1960**, *4*, 385–390.
29. Woś, A. *Klimat Polski*; Wydawn Naukowe PWN: Warszawa, Poland, 1999.
30. Licbarski, P. *Komentarz do Mapy Hydrograficznej Polski w Skali 1:50,000, Arkusz 325.1 Pruszcz Gdański*; GUGiK: Warszawa, Poland, 1989.
31. Jereczek-Korzeniewska, K. *Komentarz do Mapy Hydrograficznej Polski w Skali 1:50,000, Arkusz N-34-49-D Gdańsk-Osowa*; GUGiK: Warszawa, Poland, 2005.
32. Owaczarek, M.; Filipiak, J. Contemporary changes of thermal conditions in. 2016. Poland, 1951–2015. *Bull. Geography. Phys. Geogr. Ser.* **2016**, *10*, 31–50. [[CrossRef](#)]
33. Petelski, K.; Staszek, W. The Detailed Geological Map of Poland in Scale 1:50,000. Rumia 15. PGI–NRI. 2001. Available online: <http://baza.pgi.gov.pl> (accessed on 8 January 2022). (In Polish)
34. Pikies, R. The Detailed Geological Map of Poland in Scale 1:50,000. Żukowo 26. PGI–NRI. 2001. Available online: <http://baza.pgi.gov.pl> (accessed on 8 January 2022). (In Polish)
35. Koutaniemi, L.; Rachocki, A. Palaeohydrology and landscape development in the middle course of the Radunia basin, North Poland. *Fenn. Int. J. Geogr.* **1981**, *159*, 335–342.
36. Błaszkiwicz, M.; Piotrowski, J.A.; Brauer, A.; Gierszewski, P.; Kordowski, J.; Kramkowski, M.; Lamparski, P.; Lorenz, S.; Noryśkiwicz, A.M.; Ott, F.; et al. Climatic and morphological controls on diachronous postglacial lake and river valley evolution in the area of Last Glaciation, northern Poland. *Quat. Sci. Rev.* **2015**, *109*, 13–27. [[CrossRef](#)]
37. Kühn, B. *Geologische Spezialkarte von Preußen und den Thüringischen Staaten. Maßstab 1:25,000*; Zuckau, B., Ed.; Königlich Preussische Geologische Landesanstalt/Staatsbibliothek: Berlin, Germany, 1905.
38. Blockus, M. *Ekspertryza Techniczna Dotycząca Osuwiska w Rejonie Miejscowości Rutki w Powiecie Kartuskim, w Gminie Żukowo nad Radunią, Woj. Pomor. Gdańsk*, Poland, 2019.
39. Lidzbarski, M.; Potrykus, D.; Tarnawska, E.; Szelewicka, A.; Pasierowska, B.; Kowalewski, T. *Studium Możliwości Weryfikacji Istniejącej strefy Ochronnej Ujęcia Wody “Straszyn”*; PGI–NRI: Warszawa, Poland, 2019.
40. Świstulski, D. Zabytkowe obiekty o tematyce elektrotechnicznej w województwie pomorskim. *Zesz. Nauk. Wydziału Elektrotech. Autom. Politech. Gdańskiej* **2013**, *35*, 45–49.
41. Kulczykowski, M. Metoda gwoździowania w warunkach awarii konstrukcji oporowych. In Proceedings of the Wyd Konferencji Naukowo-Technicznej “Awary Budowlane ‘96”, Szczecin, Poland, 22–25 May 1996; Volume 2, pp. 475–482.
42. Kulczykowski, M.; Przewłocki, J.; Konarzewska, B. Application of soil nailing technique for protection and preservation historical buildings. *IOP Conf. Ser. Mater. Sci. Eng.* **2017**, *245*, 022055. [[CrossRef](#)]
43. Jereczek, K.; Rolka, A.M.; Szudarowski, W. Zbiornik Rutki jako basen sedimentacyjny. The Rutki reservoir as a depositional basin (in Polish with English summary). *Przegląd Geogr.* **1997**, *69*, 149–155.
44. Karwik, A. *Baza danych GIS Mapy Hydrogeologicznej Polski 1:50,000. Pierwszy Poziom Wodonośny, Występowanie i Hydrodynamika*; PIG–PIB: Warszawa, Poland, 2006. Available online: <https://geolog.pgi.gov.pl/> (accessed on 10 January 2023). (In Polish)
45. Tarnawska, E. *Baza danych GIS Mapy Hydrogeologicznej Polski 1:50,000. Pierwszy Poziom Wodonośny, Występowanie i Hydrodynamika*. In *Arkusz Dzierżazno*; PGI–NRI: Warszawa, Poland; PIG–PIB: Warszawa, Poland, 2011; Volume 54. Available online: <https://geolog.pgi.gov.pl/> (accessed on 8 January 2022). (In Polish)
46. Staszek, W. *Komentarz do Mapy Hydrograficznej Polski w Skali 1:50,000, Arkusz N-34-61-B Kolbudy Górne*; GUGiK: Warszawa, Poland, 2005.
47. Widernik, M. Magistrala węglowa Śląsk—Gdynia i jej znaczenie w okresie międzywojennym. *Zap. Hist.* **1984**, *2*, 31–52.
48. Fałtynowicz, W.; Królak, D. Lichens of the nature reserve “Jar Rzeki Raduni” in the Kaszubskie Lake District (Northern Poland). *Acta Bot. Cassubica* **2001**, *2*, 133–141.
49. Pawalczyk, P. Ochrona procesów generowanych przez rzeki jako podstawa ochrony przyrody w ich dolinach. *Przegląd Przyr.* **VI** **1995**, *3*, 235–255, (In Polish with English Summary).
50. Schrötter, F.L. 1796–1802. *Karte von Ost-Preussen nebst Preussisch Litthauen und West-Preussen nebst dem Netzdistrict aufgenommen unter Leitung des Königl. Preuss. Staats Ministers Frey Herrn von Schroetteer in den Jahren von 1796 bis 1802*; Staatsbibliothek zu Berlin: Berlin, Germany, 1812.
51. Stempel. *Urmessstischblatt, Topographische Karte, Maßstab 1:25,000, Blatt Zuckau*; Staatsbibliothek: Berlin, Germany, 1862.
52. Breia, M. *Situations Plan des Radyne Flusses Section III, von Babebthal bis Zuckau. Vermessen 1859 vom Feldmesser Buchwald, Gezeichnet 1860 vom Feldmesser Guth. Cpirt im Mai 1881 durch M. Breia Regierungsgs Geometer*; Archiwum Państwowe w Gdańsku: Gdańsk, Poland, 1881.
53. *Messstischblatt. Topographische Karte, Maßstab 1:25,000, Blatt Zuckau*; Staatsbibliothek: Berlin, Germany, 1900.
54. Blockus, M.; Gast, M. *Projekt Budowlany Prac Naprawczych w Rejonie Osuwiska Rutki w Gminie Żukowo nad Radunią na Działkach nr 85/1; 84/2; 85/1; 157/4*; Gdańsk, Poland, 2019.

55. Frydel, J.; Mil, L.; Szarafin, T.; Koszka-Maróń, D.; Przyłucka, M. Zmienność czasowa i zróżnicowanie przestrzenne wielkości i tempa erozji klifu Zatoki Usteckiej w rejonie Orzechowa. *Landf. Anal.* **2017**, *34*, 3–14. [CrossRef]
56. Wódka, M. Conditions of landslide development during the last decade in the Rożnów Dam-Lake region (Southern Poland) based on Airborne Laser Scanning (ALS) data analysis. *Geol. Q.* **2022**, *66*, 66. [CrossRef]
57. Itasca, C.G. *FLAC 7.0 Manual*; Minneapolis, MN, USA, 2011; Available online: <https://docs.itascacg.com/flac3d700/flac3d/docproject/source/modeling/introduction/guidetohelp.html> (accessed on 8 January 2022).
58. Chung, C.F.; Fabbri, A.G. Validation of spatial prediction models for landslide hazard mapping. *Nat. Hazards* **2003**, *30*, 451–472. [CrossRef]
59. Wang, Y.; Feng, L.; Li, S.; Ren, F.; Du, Q. A hybrid model considering spatial heterogeneity for landslide susceptibility mapping in Zhejiang Province, China. *Catena* **2020**, *188*, 104425. [CrossRef]
60. Wiegand, T. Modellierung von Massenverlagerungen und ihre Darstellung in Gafahrungskarten auf Blatt 7719 Balingen mit Hilfe von Geoinformationssystemen (GIS). *Angew. Geogr. Informationsverarbeitung VIII Salzburger Geogr. Mater.* **1996**, *24*.
61. Ayalew, L.; Yamagishi, H.; Marui, H.; Kanno, T. Landslides in Sado Island of Japan: Part II. GIS-based susceptibility mapping with comparisons of results from two methods and verifications. *Eng. Geol.* **2005**, *81*, 432–445. [CrossRef]
62. Trigila, A.; Iadanza, C.; Esposito, C.; Scarascia-Mugnozza, G. Comparison of logistic regression and random forests techniques for shallow landslide susceptibility assessment in Giampilieri (NE Sicily, Italy). *Geomorphology* **2015**, *249*, 119–136. [CrossRef]
63. Bai, S.; Lu, P.; Wang, J. Landslide susceptibility assessment of the Youfang catchment using logistic regression. *J. Mt. Sci.* **2015**, *12*, 816–827. [CrossRef]
64. Lee, S.; Woo, J.; Kwan-Young, O.; Moun-Jin, L. The spatial prediction of landslide susceptibility applying artificial neural network and logistic regression models: A case study of Indie, Korea. *Open Geosci.* **2016**, *8*, 117–132. [CrossRef]
65. Hemasinghe, H.; Rangali, R.S.S.; Deshapriya, N.L.; Samarakoon, L. Landslide susceptibility mapping using logistic regression model (a case study in Badulla District, Sri Lanka). *Procedia Eng.* **2018**, *212*, 1046–1053. [CrossRef]
66. Lee, S. Application of likelihood ratio and logistic regression models to landslide susceptibility mapping using GIS. *Environ. Manag.* **2004**, *34*, 223–232. [CrossRef] [PubMed]
67. Rasyid, A.R.; Bhandary, N.P.; Yatabe, R. Performance of frequency ratio and logistic regression model in creating GIS based landslides susceptibility map at Lompobattang Mountain, Indonesia. *Geoenviro. Disasters* **2016**, *3*, 19. [CrossRef]
68. Oh, H.-J.; Kadavi, P.R.; Lee, C.-W.; Lee, S. Evaluation of landslide susceptibility mapping by evidential belief function, logistic regression and support vector machine models. *Geomat. Nat. Hazards Risk* **2018**, *9*, 1053–1070. [CrossRef]
69. Małka, A. GIS-Based Landslide Susceptibility Modelling in Urbanized Areas: A Case Study of the Tri-City Area of Poland. *GeoHazards* **2022**, *3*, 508–528. [CrossRef]
70. Hilbe, J.M. *Logistic Regression Models*; Chapman and Hall/CRC Press: New York, NY, USA, 2009.
71. Bui, D.T.; Lofman, O.; Revhaug, I.; Dick, O. Landslide susceptibility analysis in the Hoa Binh province of Vietnam using statistical index and logistic regression. *Nat. Hazards* **2011**, *59*, 1413–1444. [CrossRef]
72. Zêzere, J.L.; Pereira, S.; Melo, R.; Oliveira, S.C.; Garcia, R.A.C. Mapping landslide susceptibility using data-driven methods. *Sci. Total Environ.* **2017**, *589*, 250–267. [CrossRef]
73. Pamela; Sadisun, I.A.; Arifianti, Y. Weights of evidence method for landslide susceptibility mapping in Takengon, Central Aceh, Indonesia. *IOP Conf. Ser. Earth Environ. Sci.* **2018**, *118*, 012037. [CrossRef]
74. Varnes, D.J. Slope movement types and processes. In *Landslides, Analysis and Control*; Schuster, R.L., Krizek, R.J., Eds.; Special report 176: Transportation research board; National Academy of Sciences: Washington, DC, USA, 1978; pp. 11–33.
75. Cruden, D.M.; Couture, R. The working classification of landslides: Material matters. In Proceedings of the 64th and 14th Pan-American conference on soil mechanics and geotechnical engineering, Toronto, ON, Canada, 2–6 October 2011; Available online: <http://geoserver.ing.puc.cl/info/conferences/> (accessed on 8 January 2020).
76. Hungr, O.; Leroueil, S.; Picarelli, L. The Varnes classification of landslide types, an update. *Landslides* **2014**, *11*, 167–194. [CrossRef]
77. Dikau, R.; Brunsden, D.; Schrott, L.; Ibsen, M.L. Landslide Recognition. In *Identification, Movement and Causes*; International Association of Geomorphologists; John Wiley and Sons: Chichester, UK, 1996.
78. Swets, J.A. Measuring the accuracy of diagnostic systems. *Science* **1988**, *240*, 1285–1293. [CrossRef] [PubMed]
79. Mrozek, T.; Laskowicz, I.; Zabuski, L.; Kulczykowski, M.; Świdziński, W. Landslide susceptibility and risk assessment in a non-mountainous region—A case study of Koronowo, Northern Poland. *Geol. Q.* **2016**, *60*, 758–769. [CrossRef]
80. Małka, A. Podatność i ryzyko osuwiskowe w obszarach rzeźby młodoglacjalnej, przeobrażonej antropogenicznie, na terenie Gdyni. Pr. doktorska. *Arch. Państw. Inst. Geol. PIB* **2018**. [CrossRef]
81. Starkel, L. Złożoność czasowa i przestrzenna opadów ekstremalnych i efekty geomorfologiczne i drogi przeciwdziałania im. *Landf. Anal.* **2011**, *15*, 65–80.
82. Ossowski, P. *Odrowadzanie Wód Opadowych od Istniejącego Przepustu Zlokalizowanego w Ciągu Drogi Wojewódzkiej nr 211 w m. Borkowo Dz 74/1 Obręb 0003 Borkowo*; Zarząd Dróg Wojewódzkich w Gdańsku: Gdańsk, Poland, 2015.
83. Segoni, S.; Tofani, V.; Rosi, A.; Catani, F.; Casagli, N. Combination of Rainfall Thresholds and Susceptibility Maps for Dynamic Landslide Hazard Assessment at Regional Scale. *Front. Earth Sci.* **2018**, *6*, 85. [CrossRef]
84. Mondini, A.C.; Guzzetti, F.; Chang, K.-T.; Monserrat, O.; Martha, T.R.; Manconi, A. Landslide failures detection and mapping using Synthetic Aperture Radar: Past, present and future. *Earth-Sci. Rev.* **2021**, *216*, 103574. [CrossRef]

85. Jakob, M. The impacts of logging on landslide activity at Clayoquot Sound, British Columbia. *CATENA* **2000**, *38*, 279–300. [CrossRef]
86. Cannon, S.H.; Gartner, J.E. Wildfire-related debris flow from a hazards perspective. In *Debris-Flow Hazards and Related Phenomena*; Springer Praxis Books; Springer: Berlin/Heidelberg, Germany, 2005; pp. 363–385.
87. Małka, A. Landslide susceptibility modelling using the index method and high-resolution airborne laser scanning data (LIDAR) in the area of Gdańsk. *Przegląd Geol.* **2015**, *63*, 301–311. Available online: <https://www.pgi.gov.pl> (accessed on 8 January 2022). (In Polish with English Summary).
88. Wysokiński, L. Osuwisko w Brzeźnie powstałe w wyniku prac geofizycznych. *Przegląd Geol.* **1979**, *8*, 444–446.
89. Banach, M. Zmiany jeziora Brzeźno po katastrofie w 1976 roku. *Śląskie Pr. Geogr.* **2005**, *2*, 113–220.
90. Jiao, J.J.; Wang, X.-S.; Nandy, S. Confined groundwater zone and slope instability in weathered igneous rocks in Hong Kong. *Eng. Geol.* **2005**, *80*, 71–92. [CrossRef]
91. Montgomery, D.R.; Dietrich, W.E. Where do channels begin. *Nature* **1988**, *336*, 232–234. [CrossRef]
92. Grabowska-Olszewska, B. An influence of swelling on microstructural changes of bentonites studied with ESEM. *Przegląd Geol.* **2001**, *49*, 299–302. Available online: <https://www.pgi.gov.pl> (accessed on 8 January 2022). (In Polish with English Summary).
93. Grabowski, D.; Laskowicz, I.; Małka, A.; Rubinkiewicz, J. Geoenvironmental conditioning of landsliding in river valleys of lowland regions and its significance in landslide susceptibility assessment: A case study in the Lower Vistula Valley, Northern Poland. *Geomorphology* **2022**, *419*, 108490. [CrossRef]
94. Vakhshoori, V.; Zare, M. Landslide susceptibility mapping by comparing weight of evidence, fuzzy logic, and frequency ratio methods Geomatics. *Nat. Hazards Risk Vol.* **2016**, *7*, 1731–1752. [CrossRef]
95. Arabameri, A.; Saha, S.; Roy, J.; Chen, W.; Blaschke, T.; Bui, D.T. Landslide Susceptibility Evaluation and Management Using Different Machine Learning Methods in The Gallicash River Watershed, Iran. *Remote Sens.* **2020**, *12*, 475. [CrossRef]
96. Pawluszek, K.; Borkowski, A. Impact of DEM-derived factors and analytical hierarchy process on landslide susceptibility mapping in the region of Roznow Lake, Poland. *Nat. Hazards* **2016**, *86*, 919–952. [CrossRef]
97. Perkins, J.P.; Reid, M.E.; Schmidt, K.M. Control of landslide volume and hazard by glacial stratigraphic architecture, northwest Washington State, USA. *Geology* **2017**, *45*, 1139–1142. [CrossRef]
98. Hjølstrom, F. Studies of the morphological activity of rivers as illustrated by the river Fyris. *Bull. Geol. Inst. Upps.* **1935**, *25*, 221–527.
99. Persichillo, M.G.; Bordoni, M.; Meisina, C.; Bartelletti, C.; Barsanti, M.; Giannecchini, R.; D’Amato Avanzi, G.; Galanti, Y.; Cevasco, A.; Brandolini, P.; et al. Shallow landslides susceptibility assessment in different environments. *Geomat. Nat. Hazards Risk* **2017**, *8*, 748–771. [CrossRef]
100. Remondo, J.; González, A.; De Terán, J.R.D.; Cendrero, A.; Fabbri, A.; Chung, F. Validation of landslide susceptibility maps; examples and applications from a case study in Northern Spain. *Nat. Hazards* **2003**, *30*, 437–449. [CrossRef]
101. Xiao, T.; Yu, L.; Tian, W.; Zhou, C.; Wang, L. Reducing Local Correlations Among Causal Factor Classifications as a Strategy to Improve Landslide Susceptibility Mapping. *Front. Earth Sci.* **2021**, *9*, 781674. [CrossRef]
102. Wilson, J.P.; Gallant, J.C. (Eds.) *Terrain Analysis: Principles and Applications*; John Wiley & Sons: New York, NY, USA, 2000; pp. 1–27.
103. Vatcheva, K.P.; Lee, M.; McCormick, J.B.; Rahbar, M.H. Multicollinearity in Regression Analyses Conducted in Epidemiologic Studies. *Epidemiology* **2016**, *6*, 227. [CrossRef] [PubMed]
104. Kutner, M.; Nachtsheim, C.; Neter, J. *Applied Linear Statistical Models*, 4th ed.; McGraw-Hill: New York, NY, USA; Irwin: Huntersville, NC, USA, 2004.
105. Wojciechowski, T.; Borkowski, A.; Perski, Z.; Wójcik, A. Airborne laser scanning data in landslide studies at the example of the Zbyszyce landslide (Outer Carpathians). *Przegląd Geol.* **2012**, *60*, 95–102. Available online: <https://www.pgi.gov.pl> (accessed on 8 January 2022). (In Polish with English Summary).
106. Perski, Z.; Wojciechowski, T.; Wójcik, A.; Borkowski, A. Monitoring of landslide dynamics with LIDAR, SAR interferometry and photogrammetry. Case study of Kłodne landslide. Southern Poland. In Proceedings of the World Landslide Forum 3, Beijing, China, 2–6 June 2014.
107. Wójcik, A.; Wojciechowski, T.; Wódka, M.; Kaczorowski, J.; Kamieniarz, S.; Sikora, R.; Kułak, M.; Karwacki, K.; Warmuz, B.; Perski, Z. Development of landslide research at the Polish Geological Institute. *Przegląd Geol.* **2020**, *68*, 356–363. Available online: <https://www.pgi.gov.pl> (accessed on 8 January 2022). (In Polish with English Summary).
108. Canavesi, V.; Segoni, S.; Rosi, A.; Ting, X.; Nery, T.; Catani, F.; Casagli, N. Different Approaches to Use Morphometric Attributes in Landslide Susceptibility Mapping Based on Meso-Scale Spatial Units: A Case Study in Rio de Janeiro (Brazil). *Remote Sens.* **2020**, *12*, 1826. [CrossRef]
109. Stanley, T.; Kirschbaum, D.B. A heuristic approach to global landslide susceptibility mapping. *Nat. Hazards* **2017**, *87*, 145–164. [CrossRef]
110. Wilde, M.; Günther, A.; Reichenbach, P.; Male, J.; Hervás, J. Pan-European landslide susceptibility mapping: ELSUS Version 2. *J. Maps* **2018**, *14*, 97–104. [CrossRef]
111. Wojciechowski, T. Podatność osuwiskowa Polski. *Prz. Geol.* **2019**, *67*, 320–325, (In Polish with English Summary). [CrossRef]
112. van Westen, C.J.; Castellanos, E.; Kuriakose, S.L. Spatial data for landslide susceptibility, hazard, and vulnerability assessment: An overview. *Eng. Geol.* **2008**, *102*, 112–131. [CrossRef]

113. Soeters, R.; Van Westen, C.J. Slope instability recognition, analysis and zonation. In *Landslides, Investigation and Mitigation*; Turner, A.K., Schuster, R.L., Eds.; Transportation Research Board, National Research Council, Special Report 247; National Academy Press: Washington, DC, USA, 1996; pp. 129–177.
114. Polykretis, C.; Faka, A.; Chalkias, C. Exploring the Impact of Analysis Scale on Landslide Susceptibility Modeling: Empirical Assessment in Northern Peloponnese, Greece. *Geosciences* **2018**, *8*, 261. [[CrossRef](#)]
115. Burdziej, J.; Kunz, M. Ocena wpływu rozdzielczości i metody pozyskiwania danych wysokościowych na dokładność numerycznych modeli terenu oraz modeli spadków i ekspozycji. Estimation of resolution influence and methods of acquiring high-altitude data on the accuracy of numericterrain models and models of slopes and aspects. *Arch. Fotogram. Kartogr. Teledetekcji* **2006**, *16*, 111–123, (In Polish with English Summary).
116. Booth, D.B.; Jackson, C.R. Urbanization of aquatic systems: Degradation thresholds, stormwater detention, and the limits of mitigation. *J. Am. Water Resour. Assoc.* **1997**, *33*, 1077–1090. [[CrossRef](#)]
117. Strohbach, M.W.; Döring, A.O.; Möck, M.; Sedrez, M.; Mumm, O.; Schneider, A.-K.; Weber, S.; Schröder, B. The “Hidden Urbanization”: Trends of Impervious Surface in Low-Density Housing Developments and Resulting Impacts on the Water Balance. *Front. Environ. Sci.* **2019**, *7*, 29. [[CrossRef](#)]

Disclaimer/Publisher’s Note: The statements, opinions and data contained in all publications are solely those of the individual author(s) and contributor(s) and not of MDPI and/or the editor(s). MDPI and/or the editor(s) disclaim responsibility for any injury to people or property resulting from any ideas, methods, instructions or products referred to in the content.